NASA TECHNICAL NOTE

NASA TN D-3493

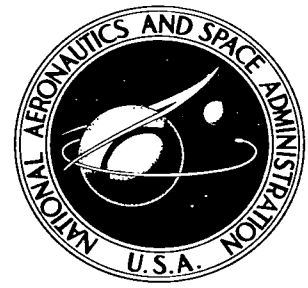

NASA TN D-3493

LOW-SPEED TESTS OF 50°-SWEPT PARAWINGS APPLIED TO A 0.17-SCALE MODEL OF A MANNED FLIGHT VEHICLE

by Frank M. Bugg

Langley Research Center
Langley Station, Hampton, Va.

NATIONAL AERONAUTICS AND SPACE ADMINISTRATION • WASHINGTON, D. C. • AUGUST 1966

LOW-SPEED TESTS OF 50°-SWEPT PARAWINGS APPLIED TO A 0.17-SCALE MODEL OF A MANNED FLIGHT VEHICLE

By Frank M. Bugg

Langley Research Center
Langley Station, Hampton, Va.

NATIONAL AERONAUTICS AND SPACE ADMINISTRATION

For sale by the Clearinghouse for Federal Scientific and Technical Information
Springfield, Virginia 22151 – Price $3.00

LOW-SPEED TESTS OF 50°-SWEPT PARAWINGS APPLIED TO A 0.17-SCALE MODEL OF A MANNED FLIGHT VEHICLE

By Frank M. Bugg
Langley Research Center

SUMMARY

A low-speed wind-tunnel investigation was made to determine the performance and control characteristics of a 0.17-scale model of a manned flight vehicle with several different parawings of 50° sweep. The effects of aspect ratio, flat-pattern sweep, leading-edge taper, trailing-edge curvature, parawing material, chord extensions, and wing position relative to the fuselage were studied.

Increasing the aspect ratio benefited the longitudinal control characteristics. The stick-force gradient with speed computed with the pivot point at the quarter-chord position of the mean aerodynamic chord on the parawing keel center line was negative (unstable) for all parawing configurations investigated and generally less negative for aspect-ratio-5.00 and -5.45 parawings than for aspect-ratio-2.57 parawings. Pivot-point locations which gave stable (positive) stick-force gradients with speed were computed for aspect-ratio-5.00 and -2.57 parawings with 45.0° flat-pattern sweep.

The use of chord extensions and increased flat-pattern sweep increased the lift-drag ratio of the model. The maximum lift-drag ratio of the model in this investigation was 4.15 and was obtained by using a modified aspect-ratio-5.45 parawing with a flat-pattern sweep of 45.0°; the maximum lift-drag ratio of this wing alone was 6.6.

INTRODUCTION

The National Aeronautics and Space Administration is engaged in a research program directed toward various applications of the parawing concept. Towed and free-flight tests have been made with unpowered, manned parawing vehicles to study the performance, stability, and control characteristics with an aspect-ratio-2.57, flat-pattern-sweep-45° parawing. (See ref. 1.) With this parawing the vehicles had low-lift-drag ratios and had unstable stick-force gradients in portions of their speed ranges. The purpose of the present investigation was to apply several different parawings to a model of one of these manned parawing vehicles in search of improved aerodynamic efficiency and improved control characteristics (stable stick-force gradients).

Aspect-ratio-2.57 and -5.00 parawings were investigated with canopy flat-pattern sweep angles of 45.0° and 47.5°. An aspect-ratio-5.45, flat-pattern-sweep-45.0° parawing was studied in its basic form, with a canard at the apex, with extended tip chords, and with a trailing-edge chord extension. Other geometric variables studied were leading-edge taper and trailing-edge curvature on the parawing flat pattern. The effects of changes in canopy material and dynamic pressure were also studied. The stick-force gradients with speed were computed for several configurations and for different pivot-point locations.

SYMBOLS

The longitudinal force and moment coefficients are presented with respect to the wind system of axes and the lateral force and moment coefficients with respect to the stability system of axes. The positive directions of force and moment coefficients and angles are shown in figure 1. The moment coefficients for the complete vehicle are given about the center of gravity (fig. 1) and the moment reference for the wing-alone data is at the 25-percent-chord point of the mean aerodynamic chord on the keel center line. Reference areas and lengths used in the reduction of data were based on the projected 50° swept wing planform, with the trailing edge taken as straight lines connecting the wing tips and the trailing edge of the root chord. These reference areas and lengths are presented in table I. The International System of Units is used with the equivalent United States customary units in parentheses.

A aspect ratio

b wing span

C_D drag coefficient, $\frac{\text{Drag}}{qS}$

C_L lift coefficient, $\frac{\text{Lift}}{qS}$

C_l rolling-moment coefficient, $\frac{\text{Rolling moment}}{qSb}$

C_m pitching-moment coefficient, $\frac{\text{Pitching moment}}{qS\bar{c}}$

C_{m_o} value at zero lift of the pitching-moment coefficient found by extrapolating the pitching-moment-coefficient curve

C_n	yawing-moment coefficient, $\frac{\text{Yawing moment}}{qSb}$
C_Y	side-force coefficient, $\frac{\text{Side force}}{qS}$
C_{l_β}	effective-dihedral parameter, $\frac{\Delta C_l}{\Delta\beta}$, per degree
C_{n_β}	directional-stability parameter, $\frac{\Delta C_n}{\Delta\beta}$, per degree
C_{Y_β}	side-force parameter, $\frac{\Delta C_Y}{\Delta\beta}$, per degree
$\bar{c}$	wing mean aerodynamic chord
D	drag
i_w	wing incidence, degree (angle between wing keel and fuselage reference line)
L	lift
L/D	lift-drag ratio
l_k	keel length
q	free-stream dynamic pressure, newtons/meters^2 (pound/foot^2)
R	free-stream Reynolds number
S	reference area of wing
V	free-stream velocity, m/sec (ft/sec)
x	distance along keel from wing apex
z	distance from keel center line measured in plane of symmetry
α	angle of attack of fuselage reference line, degree
α_k	angle of attack of wing keel, degree
β	sideslip angle, degree

ϕ wing bank angle, degree (angle of rotation of wing about wing bank axis (fig. 2) positive for right wing down)

Λ wing frame sweep, degree

Λ_o canopy flat-pattern sweep, degree

Subscripts:

max maximum

opt optimum, the value at $(L/D)_{max}$

trim measured with pitching moment equal to zero about the vehicle center of gravity

MODEL AND APPARATUS

Details of the fuselage and wing frames for the model are shown in figures 2 and 3. The wing frames were attached to the fuselage with a universal joint. The wing bank and incidence angles were set by using three control links (fig. 2). The fuselage with wing frame A (fig. 3) and the aspect ratio 2.57, $\Lambda_o = 45^o$ wing (wing 1, fig. 4) represents approximately a 0.17-scale model of vehicle B of reference 1. The overall dimensions are scaled but the structural details of the fuselage and wing-frame truss work are different for the model and vehicle B. There was no attempt made to scale structural stiffness or fabric flexibility.

The following diagram defines each wing configuration investigated and assigns to each one a number:

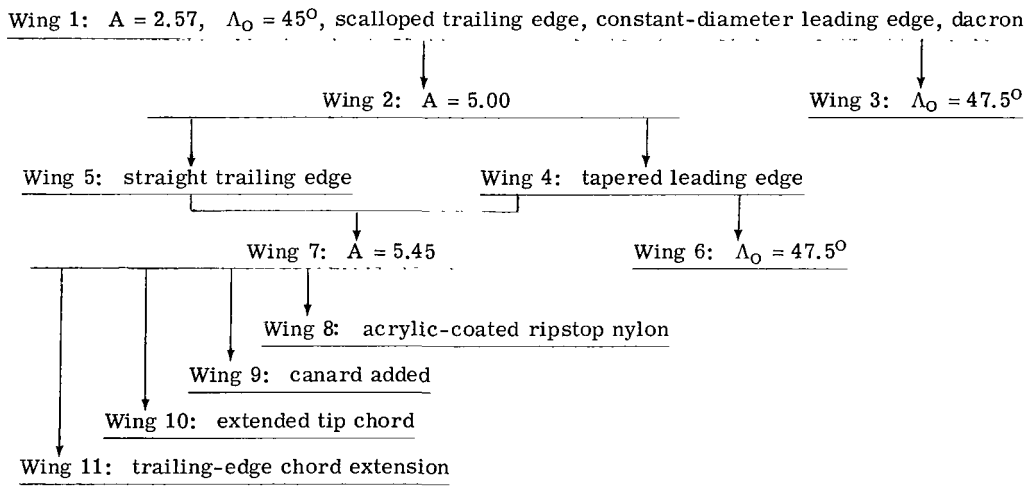

Figure 4 presents details of the canopy flat patterns and over the drawing of each are the number designations of the wings which employed that canopy. The scalloped trailing-edge wings had approximately the same flat-pattern areas as wings with straight trailing edges as indicated by the dashed lines in figure 4.

Frame C in figure 3 is shown with the canard in place at the apex and with the tip extensions used to support the tip chord and trailing-edge chord extensions. Each tip extension was made of a rod bent 40° with one end held fixed inside the leading-edge tube by means of a setscrew. With the tip deflection equal to zero, the exposed portion of each tip extension was parallel to the wing keel. Each point of a tip extension moved in an arc about the center line of the leading edge when a nonzero tip deflection was set; consequently, the wing span was increased slightly by increasing the tip deflection.

The effects of $0.2\bar{c}$ and $0.3\bar{c}$ apex covers were studied on wings 3, 6, and 7. The apex covers were dacron triangles taped to the undersurface of the wing as shown in figure 3.

The models were mounted on a sting-supported six-component strain-gage balance by means of a balance housing attached to the fuselage mounting rod. The balance housing was attached to the wing keel for the wing-alone tests. Measurements were made in the Langley high-speed 7- by 10-foot tunnel.

TESTS AND CORRECTIONS

Tests were made at dynamic pressures of 290 (6.0), 380 (8.0), 479 (10.0), 718 (15.0), and 958 (20.0) newtons per square meter (pounds per square foot) with stagnation pressure equal one atmosphere. The dynamic pressures at which the data are presented are indicated on the figures. Reynolds numbers per meter (foot) based on atmospheric conditions and free-stream velocities (1 knot = 0.5144 m/s) were as follows:

V, knots	q, N/m^2 (lb/ft^2)	R/m (R/ft)
42.7	290 (6.0)	$1.5\ (0.46) \times 10^6$
49.6	380 (8.0)	$1.7\ (0.53) \times 10^6$
55.6	479 (10.0)	$2.0\ (0.60) \times 10^6$
67.5	718 (15.0)	$2.4\ (0.73) \times 10^6$
77.9	958 (20.0)	$2.7\ (0.84) \times 10^6$

No artificial transition was used on the model.

Static longitudinal characteristics were obtained for the complete model with wings 1 and 2 at three wing pivot positions (fig. 5) and at wing-fuselage incidence angles of 0°, 10°,

15°, and 20°. Static lateral characteristics were obtained at 0° sideslip with wing bank angles of 0°, -4°, and -8° and at 0° wing bank angle with the model at sideslip angles 5° and -5°. Static longitudinal characteristics were also measured for the fuselage alone and for each of the wings in the wing-alone condition.

The data were corrected for jet boundary and blockage effects by the methods of references 2 and 3. The angles of attack were corrected for deflections of the sting and balance due to airload.

PRESENTATION OF RESULTS

The results of this investigation are presented in the figures as follows:

DISCUSSION

Static Characteristics of Complete Vehicle

Static longitudinal characteristics, A = 2.57.- The model with the A = 2.57, $\Lambda_o = 45^{\circ}$ wing (wing 1) attained a maximum L/D of about 3.6. This value was

essentially unaffected by changes in wing incidence and by changes in pivot location. (See figs. 6 to 8.) The lift curves had a constant slope of about 0.051 per degree over most of the lift range and this value also appeared to be independent of wing incidence and pivot position. The pitching-moment curves showed a sharp unstable break at wing stall.

Figure 9 presents lift coefficients and corresponding lift-drag ratios for the vehicle at $C_m = 0$. The pitching-moment data of figures 6 to 8 were extrapolated to $C_m = 0$ in some cases and the extrapolated values are the shaded points in figure 9. Increasing the wing incidence i_w moves the vehicle center of gravity rearward relative to the wing and the trim L/D is increased. The center of gravity was moved rearward by moving the pivot point rearward along the wing keel, and this procedure also increased the trim L/D at each wing incidence. Figure 5 shows the center-of-gravity location corresponding to each combination of pivot position and wing incidence for the vehicle with wing 1 and wing 2.

Static longitudinal characteristics, A = 5.00.- Figures 10, 11, and 12 show that the model reached a maximum lift-drag ratio of about 3.8 with the $A = 5.00$, $\Lambda_o = 45^o$ (wing 2). There were some small changes in the maximum value of lift-drag ratio (3.7 to 3.8) but they did not correlate with the changes in i_w or pivot location. The lift curves decreased in slope with increasing lift coefficient. The lift-curve slope C_{L_α} ranged from approximately 0.06 per degree at $C_L = 0.7$ to 0.04 per degree at $C_L = 1.3$, and there appeared to be no consistent effect of changes in the wing-fuselage orientation. This wing also produced pitching-moment curves with a sharp unstable break at wing stall. Figure 13 summarizes the lift coefficients and lift-drag ratios for the trimmed vehicle with wing 2.

Static lateral characteristics, A = 2.57.- Banking wing 1 with respect to the fuselage at $i_w = 15^o$ produced the changes in static lateral characteristics shown in figure 14. As expected, negative rolling-moment and side-force coefficients were produced by banking the wing in a negative direction. A negative wing bank produced, however, positive yawing-moment coefficients (adverse yaw). Figure 15 shows the effects of changes in sideslip on the static lateral characteristics. The static lateral derivatives for the model with wings 1 and 2 are shown in figure 18. The derivatives for the model with wing 1 indicate positive effective dihedral $\left(-C_{l_\beta}\right)$ and directional stability $\left(C_{n_\beta}\right)$ at lift coefficients below wing stall.

Static lateral characteristics, A = 5.00.- Wing 2 was banked in a negative direction (right wing up) and the resulting static lateral characteristics are shown in figure 16. The sign and general trends of the coefficients are similar to those for the vehicle with wing 1 (fig. 14). The magnitudes of the rolling- and yawing-moment coefficients produced by wing 2 for a particular bank angle are less than those produced by wing 1 for the same bank angle and at a corresponding lift coefficient but this condition is mostly due to the

way the data were nondimensionalized with different spans and the rolling moments produced by the wings were nearly equal. The effects of sideslipping the model with wing 2 are shown in figure 17. Figure 18 shows that the model with wing 2 had directional stability similar to that for the model with wing 1 and that less negative values of C_{l_β} were produced by the model with wing 2 than with wing 1 below wing stall.

Application of Wing-Alone Data To Obtain Characteristics of the Complete Vehicle

The relation between wing-alone data, fuselage wing-off data, and the data for the complete model was examined. The wing-alone data for wing 1 from figure 22 with moments transferred to the model center-of-gravity positions shown for pivot location B in figure 5 were combined with the fuselage wing-off data (fig. 19) and are presented in figure 20. Figure 21 shows a similar plot with wing-alone data for wing 2 from figure 22 transferred to the model center-of-gravity positions shown for pivot location D in figure 5 and combined with the fuselage wing-off data. Comparison of figure 20 with figure 7 shows that the combined wing 1 wing-alone and fuselage wing-off data of figure 20 closely reproduce the data for the complete model with wing 1. (The effect of q was assumed to be negligible for the purpose of this comparison.) The combined wing-alone and fuselage wing-off results of figure 21 for wing 2 are in good agreement with the results for the complete model with wing 2 (fig. 10) except that the pitching-moment coefficients on figure 21 are somewhat larger than those of figure 10.

Effects of Several Variables on Wing-Alone Characteristics

The aerodynamic efficiency of the complete model was, of course, dependent on the efficiency of the wing alone, but was severely limited by the fuselage drag as shown in a subsequent section. A positive stick-force gradient with speed for the complete model requires a positive C_{m_o} of the wing alone about the wing pivot point. (See appendix of ref. 4.) The objects of the wing-alone investigation were then to find wings with high L/D and positive C_{m_o}.

The comparisons in the above section indicate that interference effects between wing and fuselage were small. Therefore, results applicable to the complete model could be obtained from wing-alone data and the fuselage wing-off results. Figures 22 to 34 present the wing-alone data for several wing configurations and show the effects of several variables. The effects of apex covers $0.2\bar{c}$ and $0.3\bar{c}$ in length mounted as shown on frame A in figure 3 were investigated on wings 1, 3, 4, and 7; the effects were negligible except for a small increase in drag, and therefore these results are not presented.

Some of the wings were longitudinally unstable at the wing-alone moment reference but the level of longitudinal stability was much higher with the moment reference at the

vehicle center of gravity below wing stall (compare the pitching-moment curves of figures 21 and 22 for wing 2).

Effect of aspect ratio.- Figure 22 comparing wings 1 and 2 shows that a change in aspect ratio from 2.57 to 5.00 shifted the C_L for $(L/D)_{max}$ from about 0.75 to 1.25. The increase in $(L/D)_{max}$ with aspect ratio was small. Reference 5 and unpublished data also show that the increase in $(L/D)_{max}$ with aspect ratio is small for this type of wing. The canopy of wing 2 changed shape considerably at $\alpha = 16^o$. The canopy went from a generally shaky condition below $\alpha = 16^o$ to a steady condition above $\alpha = 16^o$ with canopy movement at the trailing edge only. The effects of this shape change are apparent in both the lift and pitching-moment data.

Effect of flat-pattern sweep.- The change in flat-pattern sweep from $\Lambda_o = 45^o$ for wing 1 to $\Lambda_o = 47.5^o$ for wing 3 increased the maximum lift-drag ratio from 5.4 to 6.1 (fig. 23). Wing 3 was tested at a lower angle of attack without canopy flutter than was possible with wing 1. There were no significant differences between the lift-curve slopes or the pitching-moment data for the two wings.

Figure 24 compares wing 4, $\Lambda_o = 45^o$ with wing 6, $\Lambda_o = 47.5^o$. The maximum lift-drag ratio was increased from 5.2 to 6.4 by the increase in flat-pattern sweep for these $A = 5.00$ wings. Wing 4 produced generally less negative pitching-moment coefficients than wing 6.

Effect of leading-edge taper.- The tapered leading edges were smaller at the tips than the constant diameter ones and this condition possibly improved the performance of the tip sections. Because of the extreme washout of this type of parawing (refs. 5 and 6), the tip sections probably contributed a positive increment to the pitching moment. Figure 25 shows that wing 4 with tapered leading edges had generally less negative pitching-moment coefficients than wing 2 with constant-diameter leading edges. There was little effect on $(L/D)_{max}$.

Effect of trailing-edge scallop.- Figure 26 presents the results for wing 2 with a scalloped trailing edge and wing 5 with a straight trailing edge. The stitching in the hemmed trailing edge of wing 2 shortened the trailing edge in the same way that a boltrope has been observed to shorten. The selvage of the cloth formed the trailing edge of wing 5; and thus no hem was necessary. The more negative C_m values produced by wing 2 as compared with wing 5 are typical of the change in C_m produced by boltrope shortening (ref. 7) so that the effect of scalloping the trailing edge may be masked by the effect of boltrope shortening. The straight trailing edge of wing 5 vibrated at all angles of attack with changes in the vibration frequency. The abrupt increase in drag of wing 5 at $C_L = 1.1$ may have been due to some change in the mode of canopy vibration. This same type drag increase was noted for wing 5 at several dynamic pressures. There was little effect on $(L/D)_{max}$.

Effects of $A = 5.45$ wing modifications.- The effects of a canard, tip chord extension, and trailing-edge chord extension investigated on the $A = 5.45$ wing 7 are shown in figure 27. Wing 9 with the canard had a slightly lower maximum lift-drag ratio than wing 7. Wing 10 with extended tip chords produced an $(L/D)_{max}$ of 5.5 compared with 5.2 for wing 7. In reference 6, extending the tip chord on a different type of parawing was found to increase $(L/D)_{max}$. Wing 11 with the chords extended all along the trailing edge attained a maximum L/D of 6.6. The addition of area caused changes in aspect ratio for these wings. (See table I.)

Changes in the incidence of the canard from -4.5^{o} to 7.5^{o} relative to the wing keel produced no significant change in aerodynamic characteristics of wing 9; therefore, these data are not presented. Deflecting the tips of wing 10 produced the results shown in figure 28. Raising the tips reduced the level of longitudinal stability and reduced the value of $(L/D)_{max}$. Changes in tip position for wing 11 caused the large changes in aerodynamic characteristics shown in figure 29. Raising the tips shifted the pitching-moment curves in a positive direction and caused small changes in longitudinal stability. The maximum lift-drag ratio was not affected by the change in tip deflection from -3/4 to 0; but a large reduction in $(L/D)_{max}$ accompanied further raising of the wing tip.

Effect of changes in material and dynamic pressure.- Wing 7 was made of sealed dacron material (130 gm/m^2 (3.8 oz/yd^2)) about 0.2 mm (0.006 in.) thick and wing 8 of 0.08 mm (0.003 in.) thick acrylic-coated ripstop nylon. Figure 30 shows that the lift curve was nonlinear for wing 7 and nearly linear from $C_L = 0.5$ to $C_L = 1.2$ for wing 8. Wing 8 had a higher level of longitudinal stability than wing 7 and extrapolation of the pitching-moment curves to zero lift suggested that wing 8 had a less negative C_{m_o} than wing 7. Effects of material thickness or bending stiffness similar to these effects have been seen in unpublished data for another parawing. Figures 31 to 34 show the effect of changes in dynamic pressure on wings 4, 6, and 7 with dacron canopies and wing 8 with a nylon canopy. The characteristics of wing 8 (fig. 34) appeared to be affected less by changes in dynamic pressure than the characteristics of wings 4, 6, and 7. At sufficiently high dynamic pressures the contribution of material bending stiffness in shaping the wing is believed to become negligible compared with the contribution of aerodynamic forces if frame deflections remain negligible.

Performance and Longitudinal Control Characteristics

In the wing-alone investigation several of the configurations tested had higher L/D than wing 1. Although none of the wings studied had pitching-moment curves which could be extrapolated to a positive C_{m_o}, some of the wings did have less negative extrapolated values of C_{m_o} than wing 1. Improvements in characteristics of the complete model,

using some of the more promising configurations from the wing-alone investigation, are discussed in this section.

Performance.- The lift-drag ratios for the complete model with wings 1, 3, 4, 6, and 11 were determined from wing-alone and fuselage data (figs. 19, 23, 24, and 27) and are presented in figure 35. The ideal L/D curves are presented to show the upper limit of lift-drag ratios possible for the model at each aspect ratio if the fuselage drag coefficients are as shown in figure 19. The ideal L/D values were computed with the use of the fuselage drag plus the estimated wing skin-friction drag and with the use of $C_L^2/\pi A$ as the drag due to lift. The $(L/D)_{max}$ of the model with wing 3 was about 81 percent of the $(L/D)_{max}$ for the model with an ideal aspect-ratio-2.57 wing. The model with wing 6 attained 65 percent of the maximum lift-drag ratio possible for the model with an aspect-ratio-5.00 wing. It is interesting to note that the model with wing 4 had a higher value of $(L/D)_{max}$ $\left((L/D)_{max} = 3.77\right)$, than the model with wing 1 $\left((L/D)_{max} = 3.47\right)$, whereas, in the wing-alone data $(L/D)_{max}$ for the two wings was the same. These values of L/D resulted because the fuselage drag was less at $C_{L_{opt}}$ for wing 4 than it was at $C_{L_{opt}}$ for wing 1. The maximum improvement in lift-drag ratio over that of the model with wing 1 was about 20 percent produced by wings 6 and 11 $\left((L/D)_{max} = 4.15\right.$ for wing 11$\left.\right)$.

The performance of this type vehicle could be increased further by reduction of the fuselage drag by using a streamlined structure or reduction of the importance of the fuselage drag by increasing the size of the wing relative to the fuselage. With either of these methods the drag coefficients of the fuselage would be decreased and the $(L/D)_{max}$ of the vehicle could be made to approach the $(L/D)_{max}$ of the wing alone. The ideal curves of figure 35 would then no longer represent the maximum attainable lift-drag ratios for the complete model with aspect-ratio-2.57, -5.00, and -5.45 wings.

Control characteristics.- Figure 36 presents the variation of stick force with speed for the full-scale vehicle with wings 1, 3, 4, 6, and 11. The following full-scale vehicle characteristics from reference 1 were used in computing the stick forces:

$\bar{c}$ = 2.99 m (9.80 ft)

W weight, 2850 N (640 lb)

S wing area (deployed), 12.9 m^2 (139 ft^2)

G longitudinal control gearing constant, 0.774 N/N-m (0.236 lb/lb-ft)

Stick force = $C_m q S \bar{c} G$, and C_m is pitching-moment coefficient of wing at pivot point

$$q = \frac{W \cos \gamma}{C_L S}$$

$$\gamma = \tan^{-1} \frac{D}{L}$$

The computations were made as though the wings were attached with the pivot point on the keel center line and at $\bar{c}/4$. The stick forces for the vehicle with wing 1 were also computed with the pivot at the keel center line, 47.8 percent l_k from the apex. The latter pivot position for wing 1 corresponds approximately to one of the flight-test pivot positions in reference 1. The values of C_m and C_L used in the computations were taken from figures 23, 24, and 27 at $q = 479$ N/m^2 (10.0 lb/ft^2). It is an approximation to use these values of C_m and C_L determined at a particular dynamic pressure to compute stick force through a range of dynamic pressures. The L/D values for the complete vehicle presented in figure 35 were used in computing γ. Unstable (negative) stick-force gradients were produced by all wings investigated. The stick-force gradients for the $A = 5$ and $A = 5.45$ wings showed large changes with speed and were generally less negative than those for the $A = 2.57$ wings.

The pitching-moment coefficient for the wing alone can be represented for the nonlinear curves of C_m plotted against C_L of this investigation by:

$$C_m = C_{m_{o_l}} + \frac{\partial C_m}{\partial C_L} C_L$$

where $\partial C_m/\partial C_L$ and $C_{m_{o_l}}$ for a given C_L are the slope and intercept of the tangent to the C_m curve at the given C_L. With these definitions of $C_{m_{o_l}}$ and $\partial C_m/\partial C_L$ the stick-force equation can be written:

$$\text{Stick force} = \left(\frac{C_{m_{o_l}}}{C_L} + \frac{\partial C_m}{\partial C_L} \right) (W \bar{c} G \cos \gamma)$$

where the pivot point is at the wing-alone moment reference.

The variation of $\cos \gamma$ was small (from 0.82 up to 0.97); thus, the term $W\bar{c}G \cos \gamma$ is approximately constant. The stick-force equation shows that at a particular value of C_L, a change in $\partial C_m/\partial C_L$ will cause an increment of change in stick force; a change in $C_{m_{o_l}}$ will cause a change in the slope of the curve for stick force plotted against speed, and the sign of the stick-force gradient will be the same as the sign of $C_{m_{o_l}}$. Moving the pivot point (moment reference) in a direction parallel to the wing keel from the $\bar{c}/4$ position (42.4 percent l_k) to 47.8 percent l_k produced changes in the slope $\partial C_m/\partial C_L$ of the wing-alone pitching-moment curves and the incremental change in stick force produced by this change in wing-fuselage orientation is shown in figure 36 by the curves for wing 1. For each of the small portions of the curves for wings 4, 6, and 11 in figure 36

where the stick-force gradient is positive, there is a corresponding portion of the pitching-moment curve (figs. 24 and 27) where $C_{m_{O_l}}$ is positive. $\left(C_{m_{O_l}}\right.$ is positive between $C_L = 0.5$ and 0.6 for wing 4, between $C_L = 0.4$ and 0.5 for wing 6, and between $C_L = 0.7$ and 0.8 for wing 11.$\left.\right)$

Figure 37 presents the variation of stick force with speed as computed for wings 1 and 4 for four wing positions relative to the fuselage such that the stick force is zero at $C_L = 0.9$ $\left((L/D)_{max}\right.$ occurs at $C_L = 0.9$ for wing 4$\left.\right)$. For distances between the pivot point and the keel center line of about $0.3\bar{c}$ and greater, the stick-force gradient with speed was positive for the vehicle with wing 4 ($0.3\bar{c} = 0.644$ m (2.11 ft) on the full-scale vehicle with the $A = 5$ wing). Figure 37 shows that for stable stick-force gradient with speed, the required distance between pivot point and keel center line was greater than $0.3\bar{c}$ for the vehicle with wing 1 ($0.3\bar{c} = 1.35$ m (4.41 ft) on the full-scale vehicle with the $A = 2.57$ wing).

CONCLUDING REMARKS

A low-speed wind-tunnel investigation was made to determine the performance and control characteristics of a 0.17-scale model of a manned flight vehicle with several different parawings of 50° sweep. The use of chord extensions and increased flat-pattern sweep increased the lift-drag ratio of the model. The maximum lift-drag ratio of the model in this investigation was 4.15 and was obtained using a modified aspect-ratio-5.45 parawing with flat-pattern sweep 45.0°; the maximum lift-drag ratio of this wing alone was 6.6. Reduction of the fuselage drag or reduction of the importance of the fuselage drag by increasing the wing size relative to the fuselage should be considered in addition to improvements in wing performance if the performance of the complete vehicle is to be materially increased.

Increasing the aspect ratio benefited the longitudinal control characteristics. The stick-force gradient with speed, computed with the pivot point at the quarter-chord position of the mean aerodynamic chord on the parawing keel center line, was negative (unstable) for all parawing configurations investigated and generally less negative for aspect-ratio-5.00 and -5.45 parawings than for aspect-ratio-2.57 parawings. Displacing the pivot point from the keel center line toward the vehicle center of gravity gave positive stick-force gradients with speed.

Langley Research Center,
National Aeronautics and Space Administration,
Langley Station, Hampton, Va., March 14, 1966.

REFERENCES

1. Layton, Garrison P., Jr.; and Thompson, Milton O.: Preliminary Flight Evaluation of Two Unpowered Manned Paragliders. NASA TN D-1826, 1963.

2. Gillis, Clarence L.; Polhamus, Edward C.; and Gray, Joseph L., Jr.: Charts for Determining Jet-Boundary Corrections for Complete Models in 7- by 10-Foot Closed Rectangular Wind Tunnels. NACA WR L-123, 1945. (Formerly NACA ARR L5G31.)

3. Herriot, John G.: Blockage Corrections for Three-Dimensional-Flow Closed-Throat Wind Tunnels, With Consideration of the Effect of Compressibility. NACA Rept. 995, 1950. (Supersedes NACA RM A7B28.)

4. Johnson, Joseph L., Jr.: Low-Speed Wind-Tunnel Investigation To Determine the Flight Characteristics of a Model of a Parawing Utility Vehicle. NASA TN D-1255, 1962.

5. Bugg, Frank M.: Effects of Aspect Ratio and Canopy Shape on Low-Speed Aerodynamic Characteristics of 50.0^{o} Swept Parawings. NASA TN D-2922, 1965.

6. Polhamus, Edward C.; and Naeseth, Rodger L.: Experimental and Theoretical Studies of the Effects of Camber and Twist on the Aerodynamic Characteristics of Parawings Having Nominal Aspect Ratios of 3 and 6. NASA TN D-972, 1963.

7. Croom, Delwin R.; Naeseth, Rodger L.; and Sleeman, William C., Jr.: Effects of Canopy Shape on Low-Speed Aerodynamic Characteristics of a 55^{o} Swept Parawing With Large-Diameter Leading Edges. NASA TN D-2551, 1964.

TABLE I.- PROJECTED PLANFORM GEOMETRY

[$\Lambda = 50^{o}$]

Wing	A	S, m^2 (ft^2)	$\bar{c}$, m (in.)	b, m (in.)
1, 3	2.57	0.3732 (4.017)	0.5080 (20.00)	0.9797 (38.57)
2, 4, 5, 6	5.00	.3732 (4.017)	.3642 (14.34)	1.366 (53.78)
7, 8	5.45	.3732 (4.017)	.3485 (13.72)	1.426 (56.15)
9	5.40	.3764 (4.052)	.3485 (13.72)	1.426 (56.15)
10	5.38	.3780 (4.069)	.3485 (13.72)	1.426 (56.15)
11	4.86	.4184 (4.504)	.3531 (13.90)	1.426 (56.15)

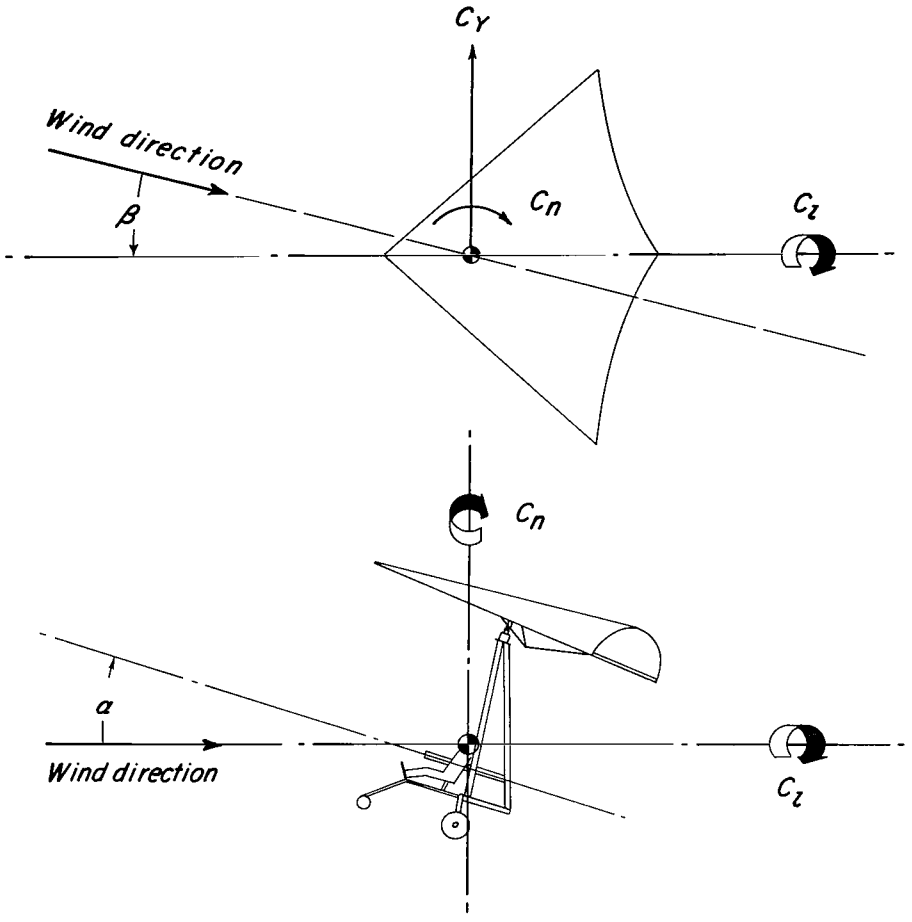

(a) Lateral.

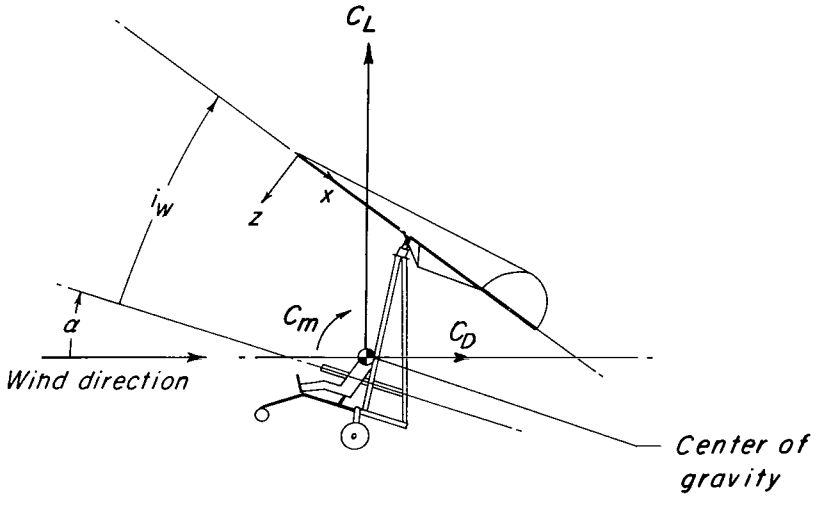

(b) Longitudinal.

Figure 1.- System of axes and convention used to define positive sense of forces, moments, and angles.

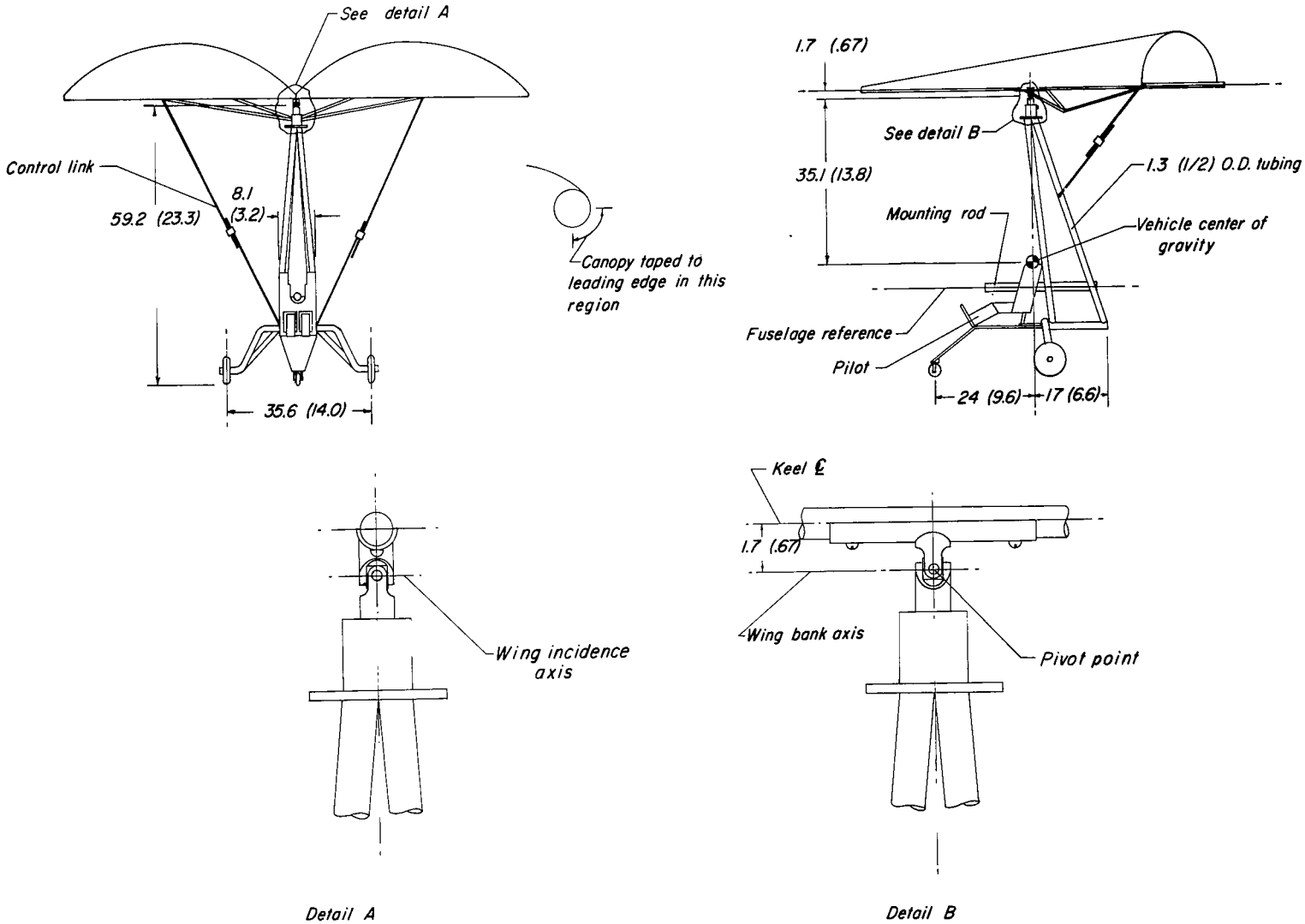

Figure 2.- Details of fuselage construction. All dimensions in cm (in.) or as noted.

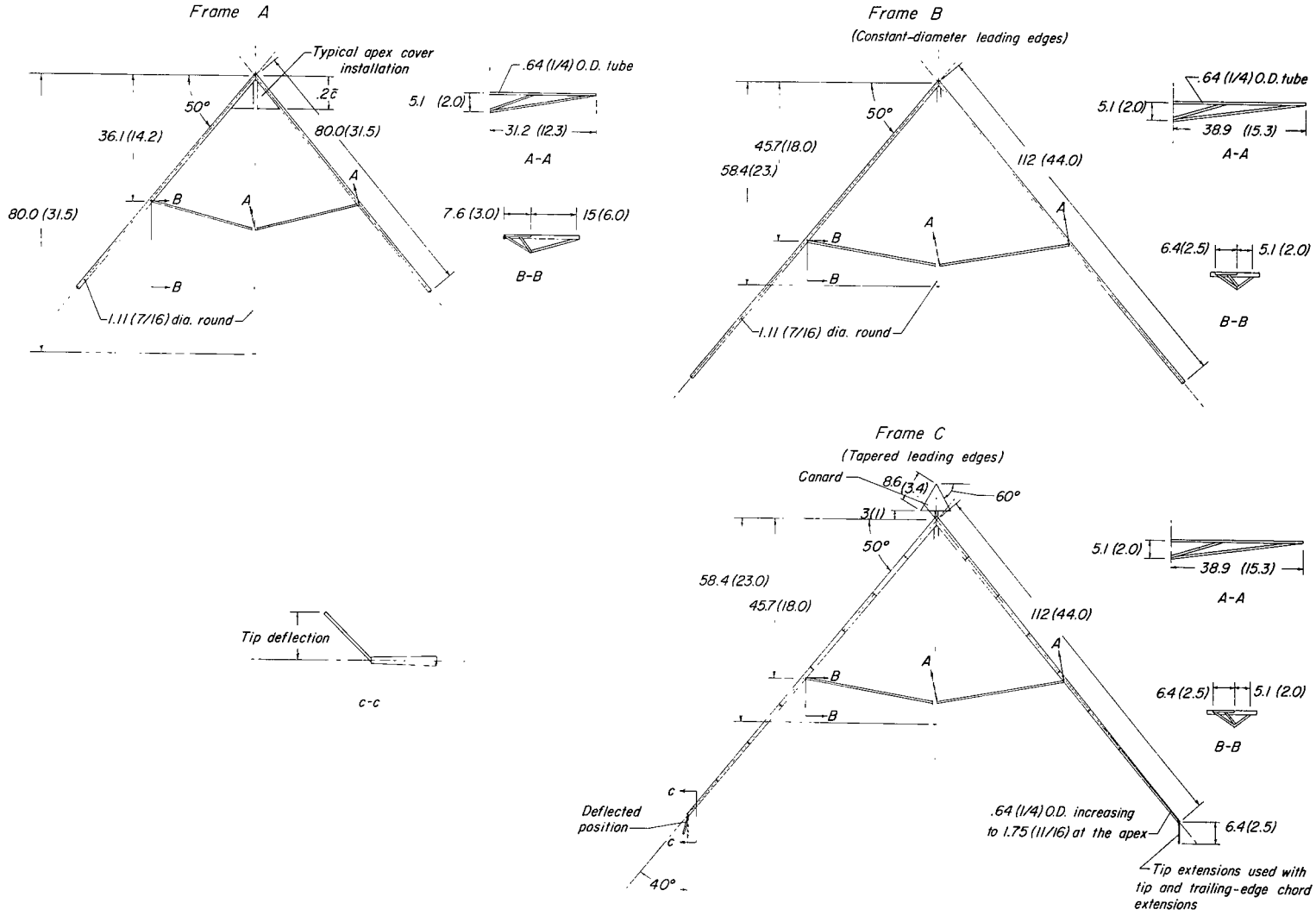

Figure 3.- Details of wing frame construction. All dimensions in cm (in.) or as noted.

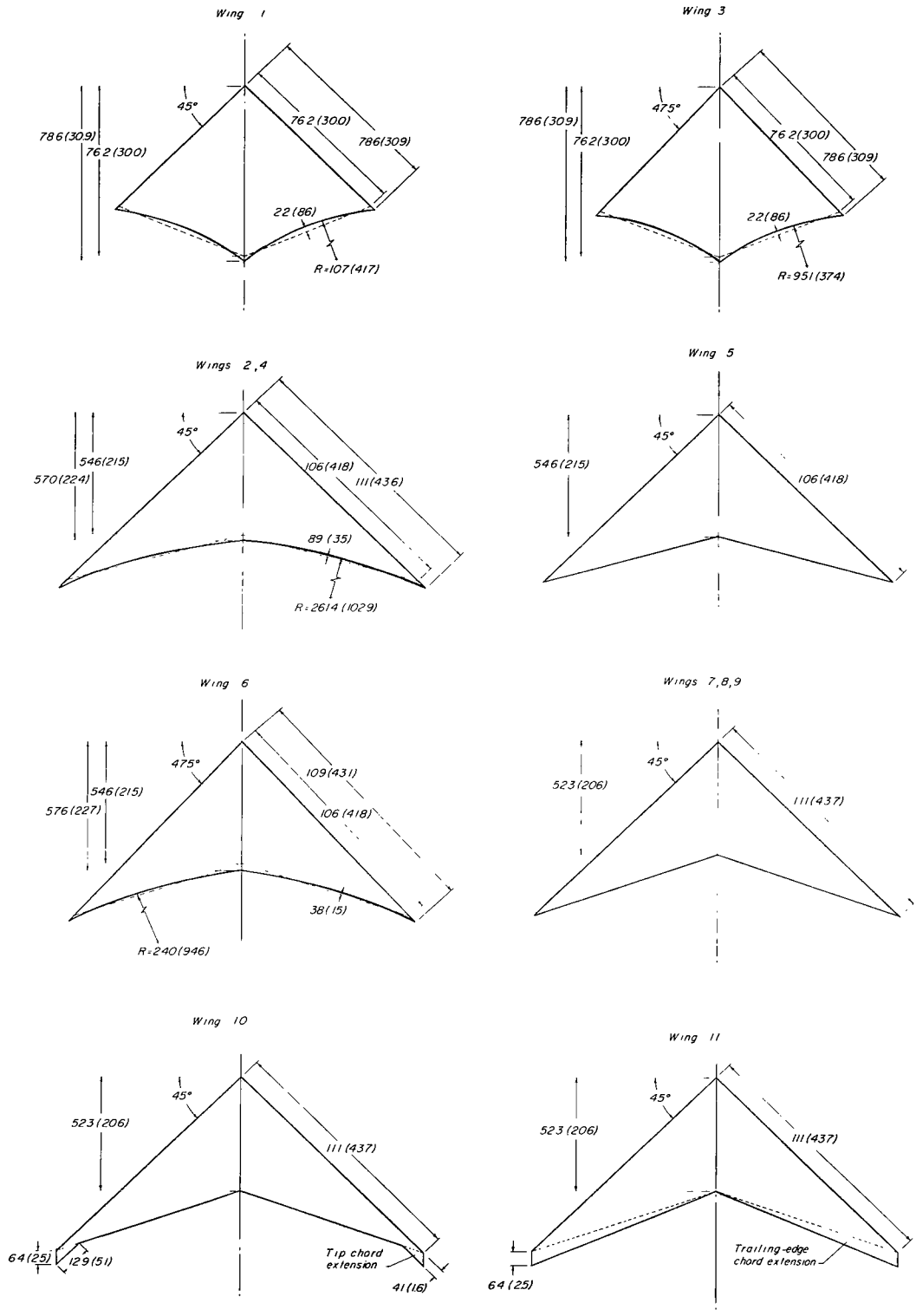

Figure 4.- Geometry of canopy flat patterns. All dimensions in cm (in.) or as noted.

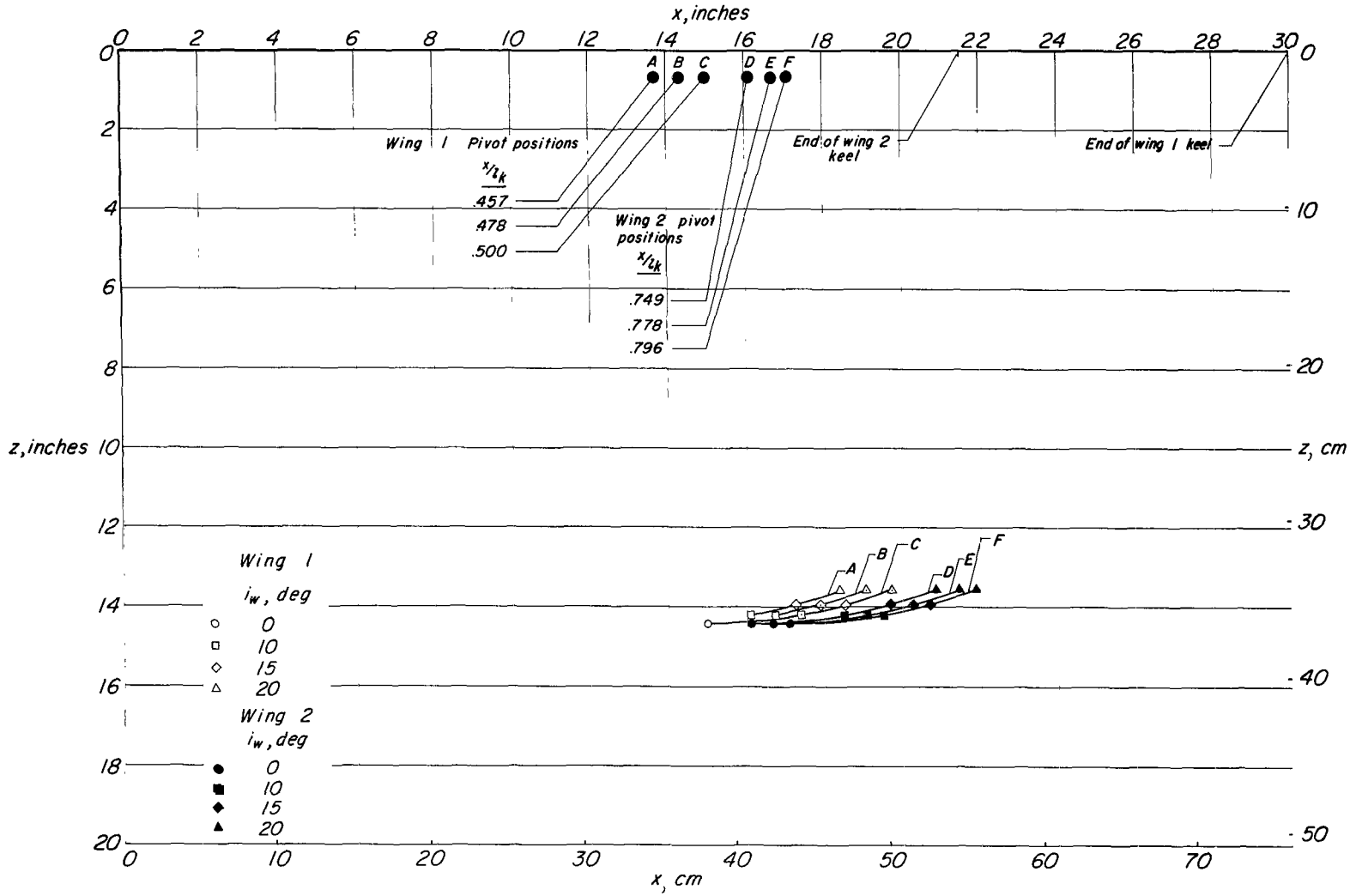

Figure 5.- Model center-of-gravity positions relative to wing 1 and wing 2.

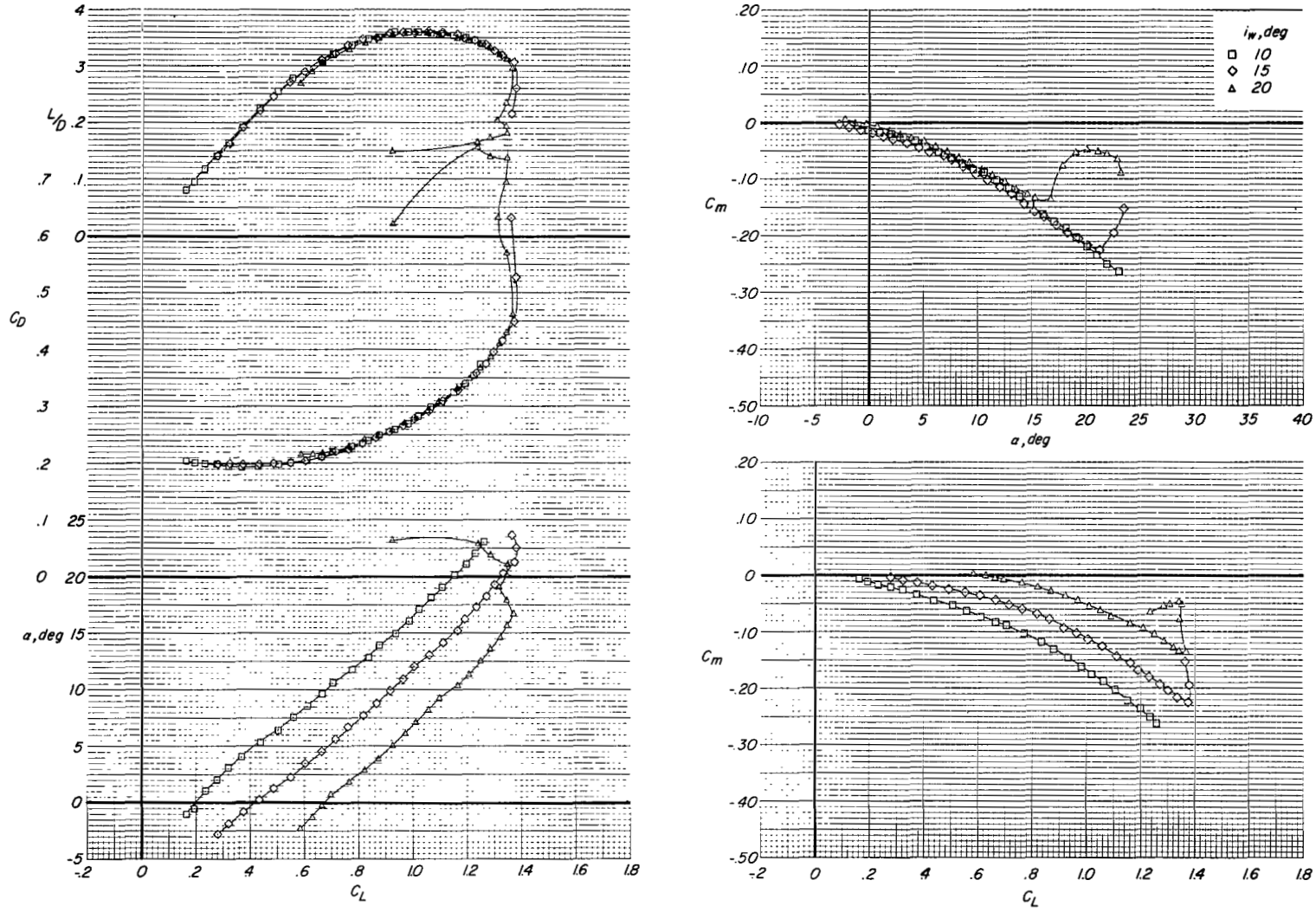

Figure 6.- Effect of wing-fuselage incidence on longitudinal aerodynamic characteristics of model with wing 1. The pivot point is at $x/l_k = 0.457$ and $z/\bar{c} = 0.033$. $q = 958\ N/m^2$ (20.0 lb/ft^2).

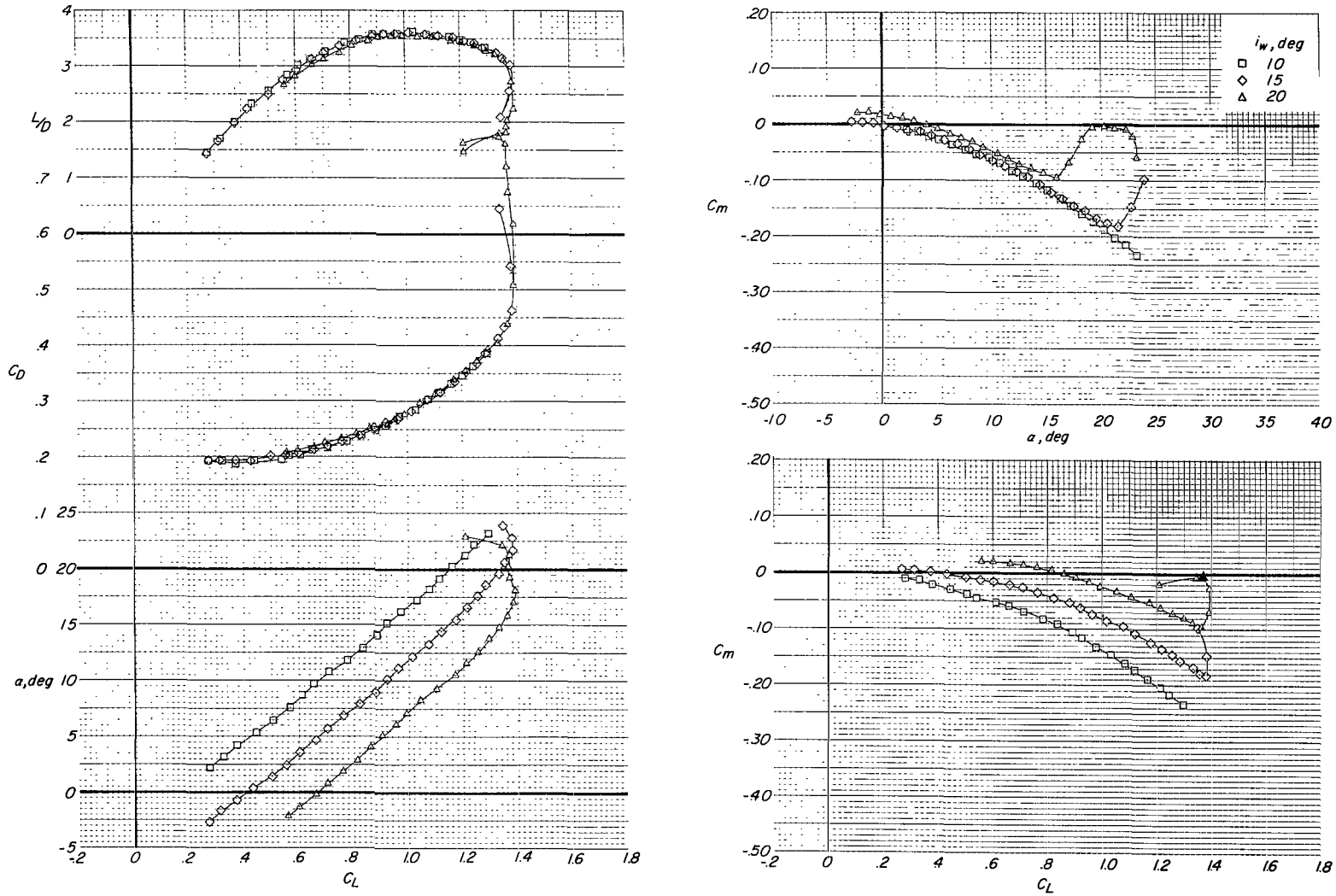

Figure 7.- Effect of wing-fuselage incidence on longitudinal aerodynamic characteristics of model with wing 1. The pivot point is at $x/\ell_k = 0.478$ and $z/\bar{c} = 0.033$. $q = 958\ N/m^2$ (20.0 lb/ft^2).

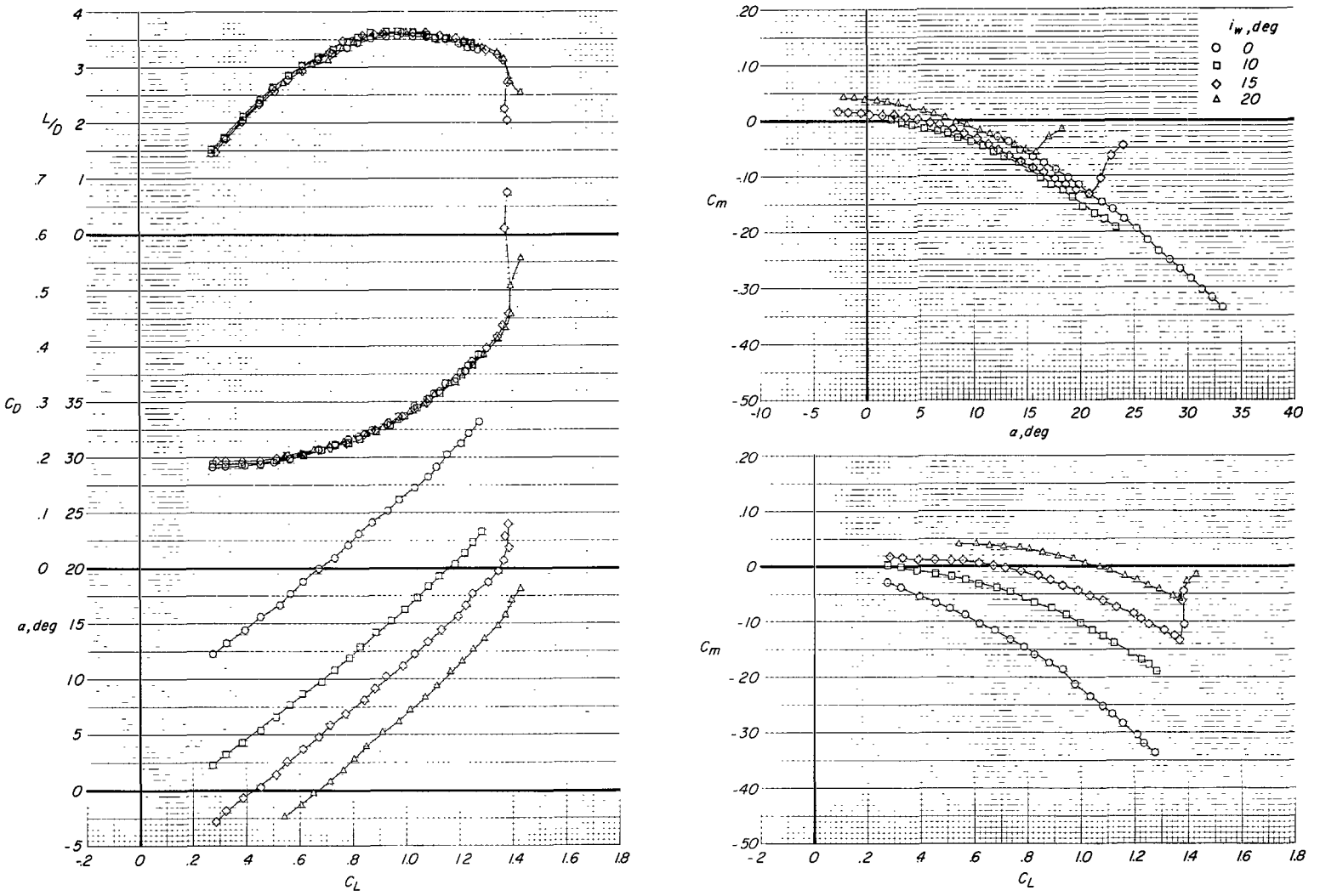

Figure 8.- Effect of wing-fuselage incidence on longitudinal aerodynamic characteristics of model with wing 1. The pivot point is at $x/l_k = 0.500$ and $z/\bar{c} = 0.033$. $q = 958\ N/m^2$ (20.0 lb/ft^2).

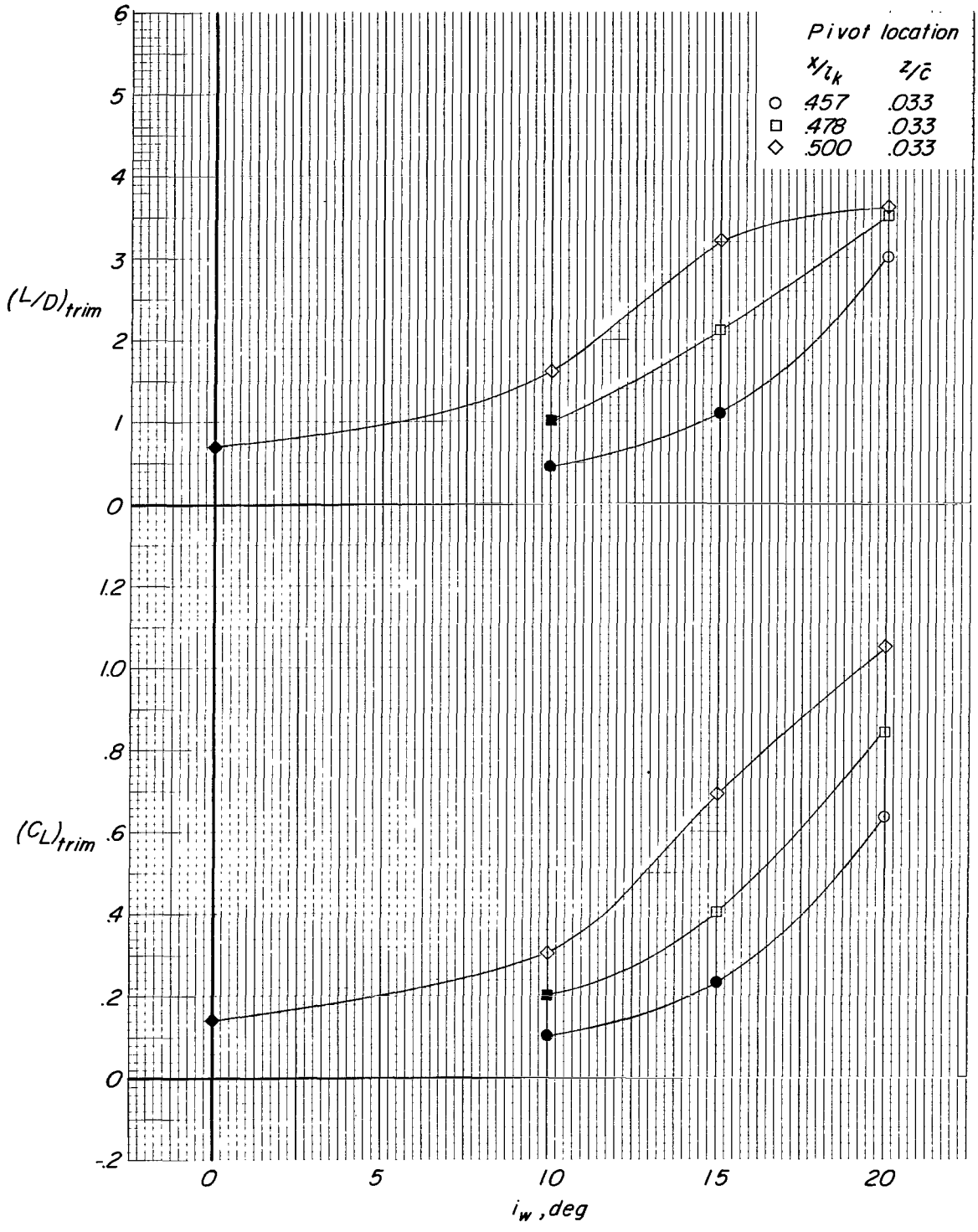

Figure 9.- Effect of wing attachment point on trimmed lift and drag characteristics of model with wing 1. $q = 958\ N/m^2$ (20.0 lb/ft^2).

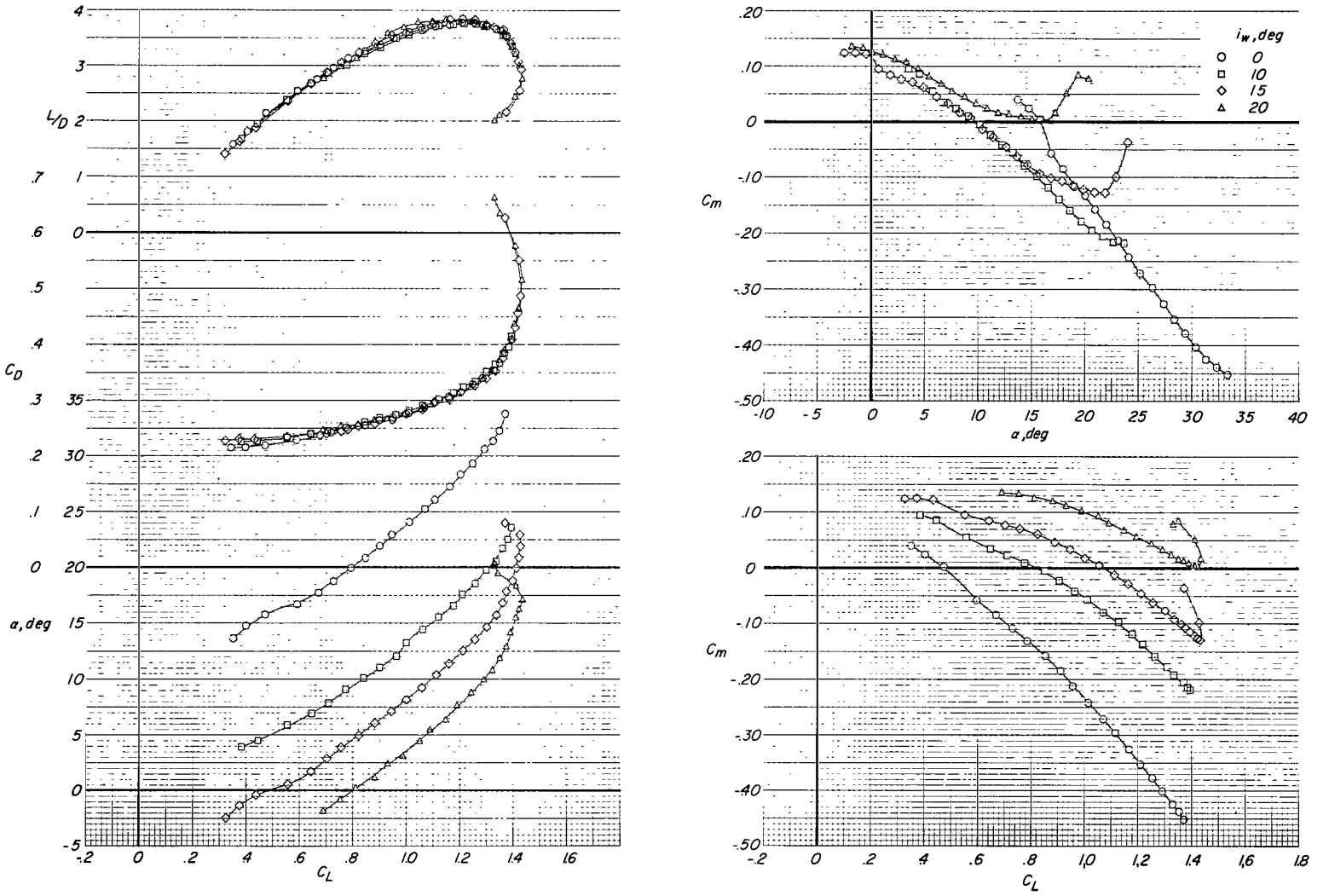

Figure 10.- Effect of wing-fuselage incidence on longitudinal aerodynamic characteristics of model with wing 2. The pivot point is at $x/l_k = 0.749$ and $z/\bar{c} = 0.047$. $q = 958\ N/m^2$ (20.0 lb/ft^2).

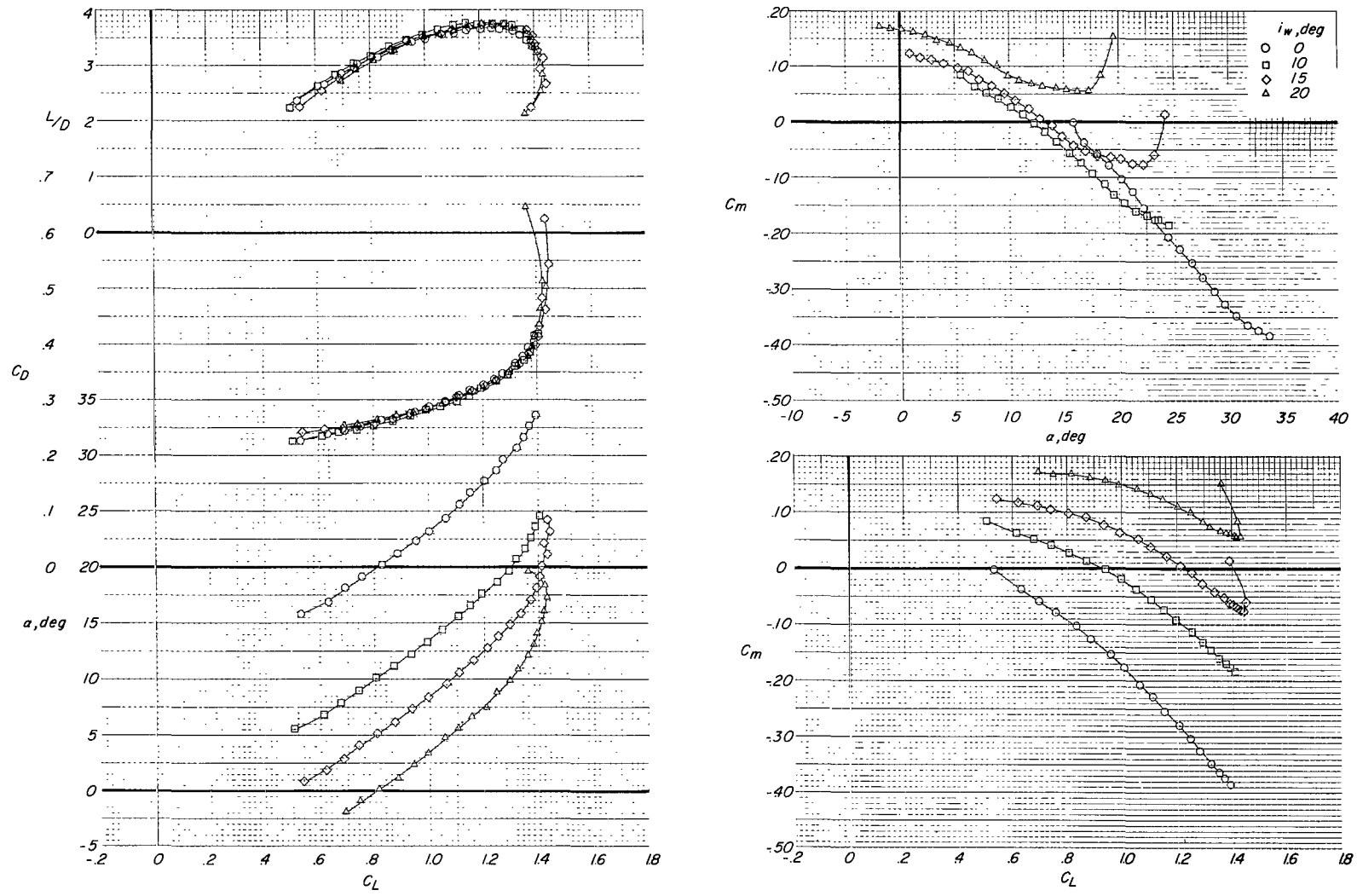

Figure 11.- Effect of wing-fuselage incidence on longitudinal aerodynamic characteristics of model with wing 2. The pivot point is at $x/l_k = 0.778$ and $z/\bar{c} = 0.047$. $q = 958\ N/m^2$ (20.0 lb/ft2).

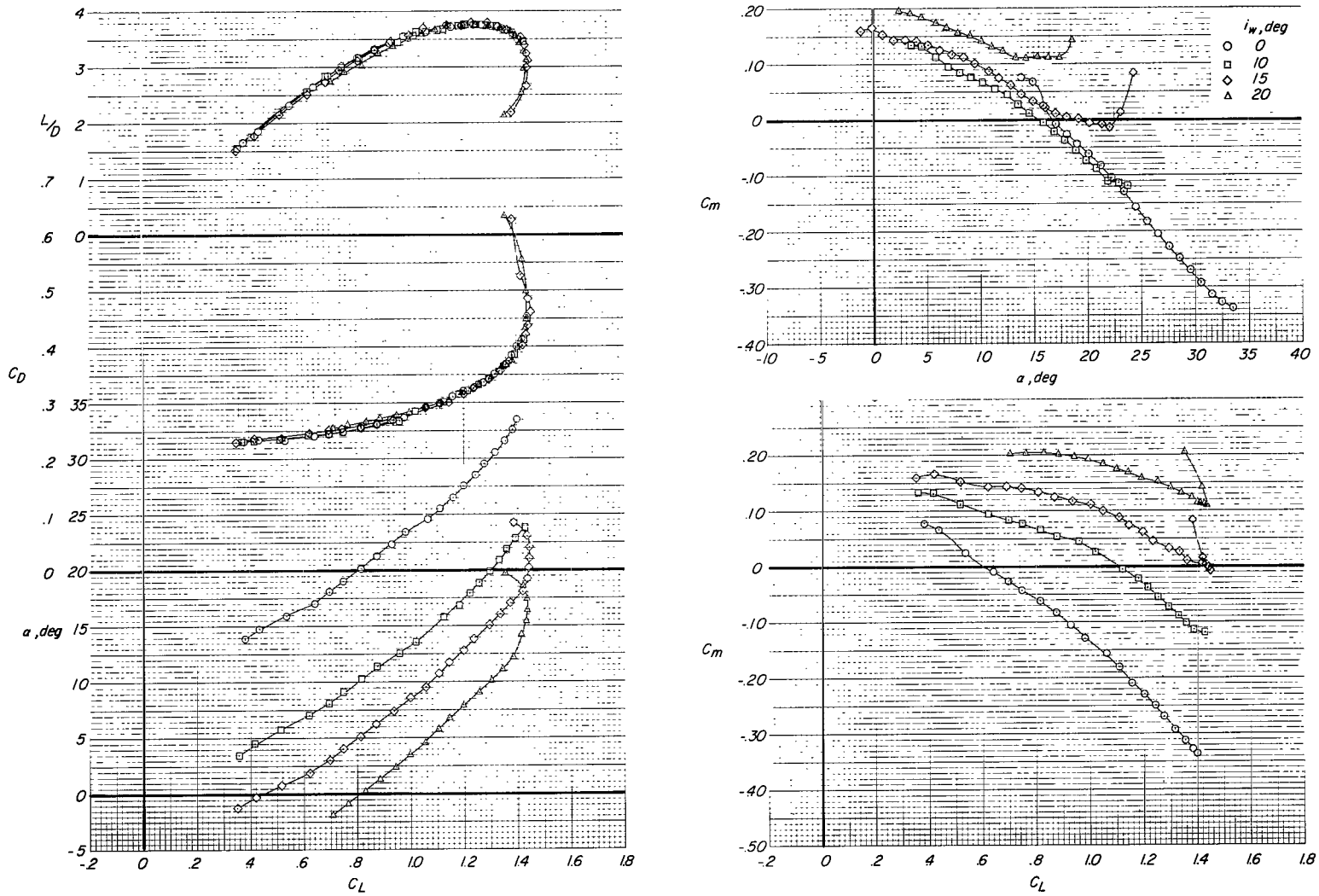

Figure 12.- Effect of wing-fuselage incidence on longitudinal aerodynamic characteristics of model with wing 2. The pivot point is at $x/l_k = 0.796$ and $z/\bar{c} = 0.047$. $q = 958\ N/m^2$ (20.0 lb/ft^2).

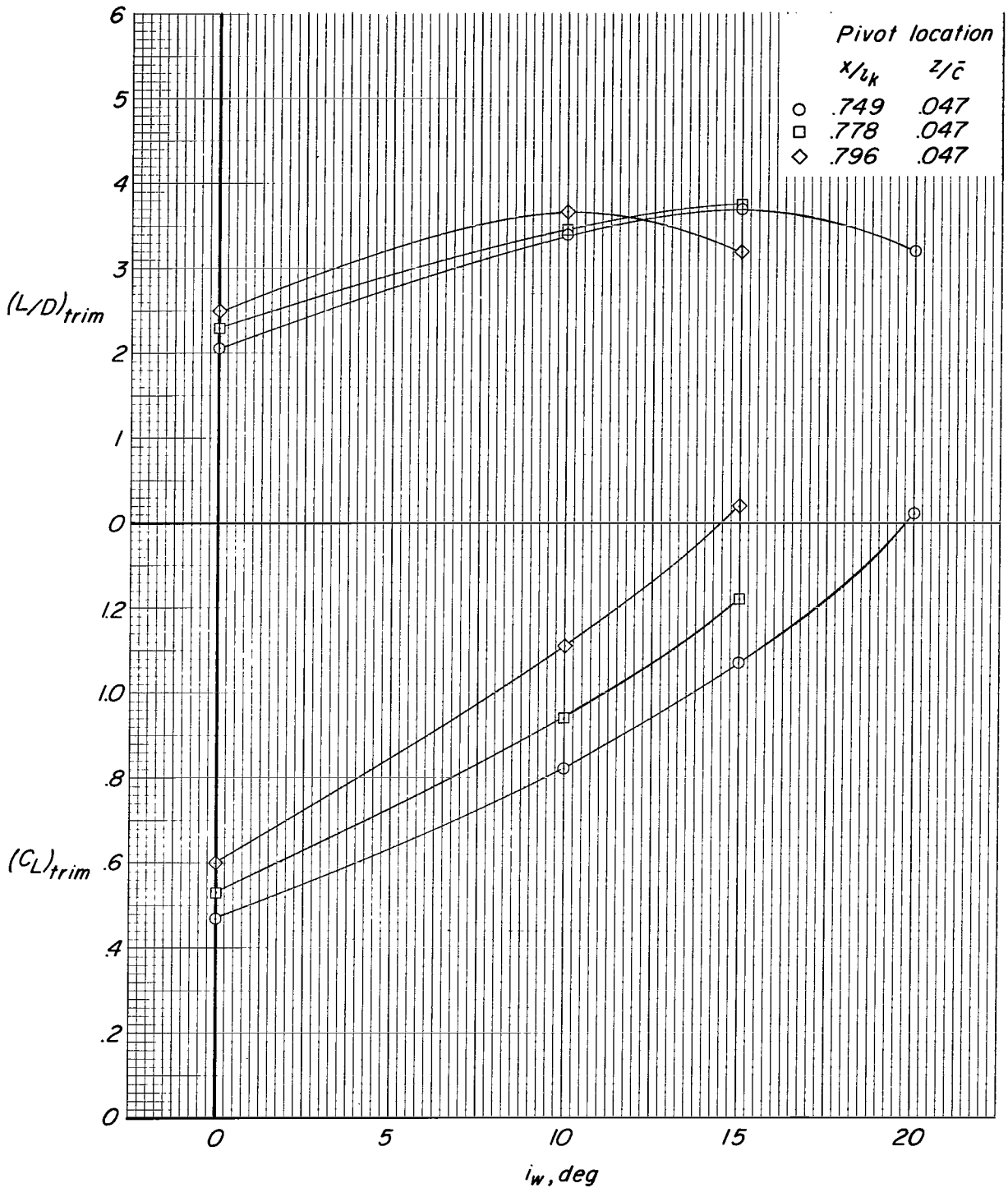

Figure 13.- Effect of wing attachment point on trimmed lift and drag characteristics of model with wing 2. $q = 958\ N/m^2$ (20.0 lb/ft^2).

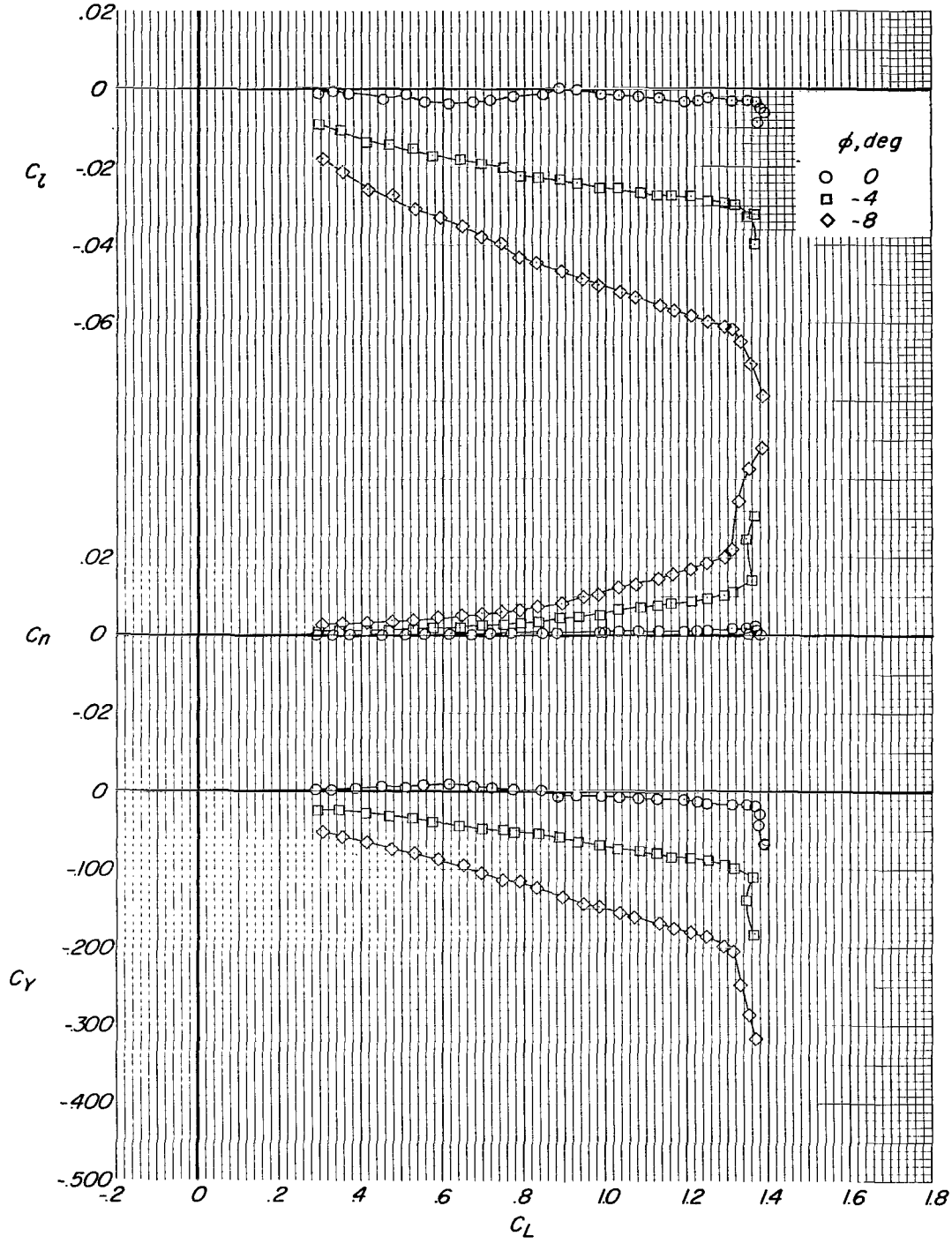

Figure 14.- Effect of wing bank angle on lateral aerodynamic characteristics of model with wing 1. Pivot location is $x/l_k = 0.500$ and $z/\bar{c} = 0.033$. Sideslip angle is 0^0; $i_w = 15^0$; and $q = 958\ N/m^2$ (20.0 lb/ft^2).

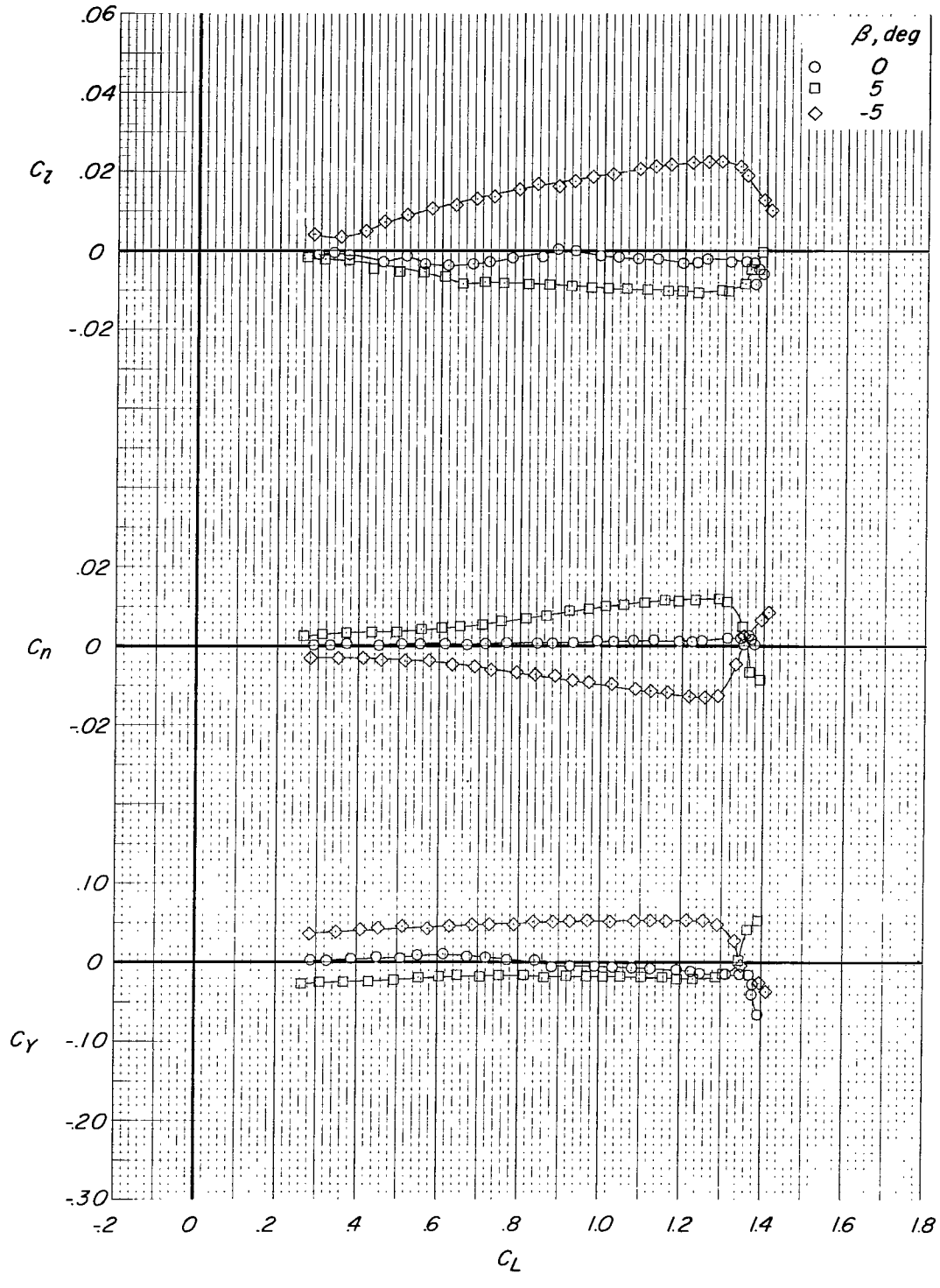

Figure 15.- Effect of sideslip angle on lateral aerodynamic characteristics of model with wing 1. Pivot location is $x/l_k = 0.500$ and $z/\bar{c} = 0.033$. Wing bank angle is 0^0; $i_w = 15^0$; and $q = 958\ N/m^2$ (20.0 lb/ft^2).

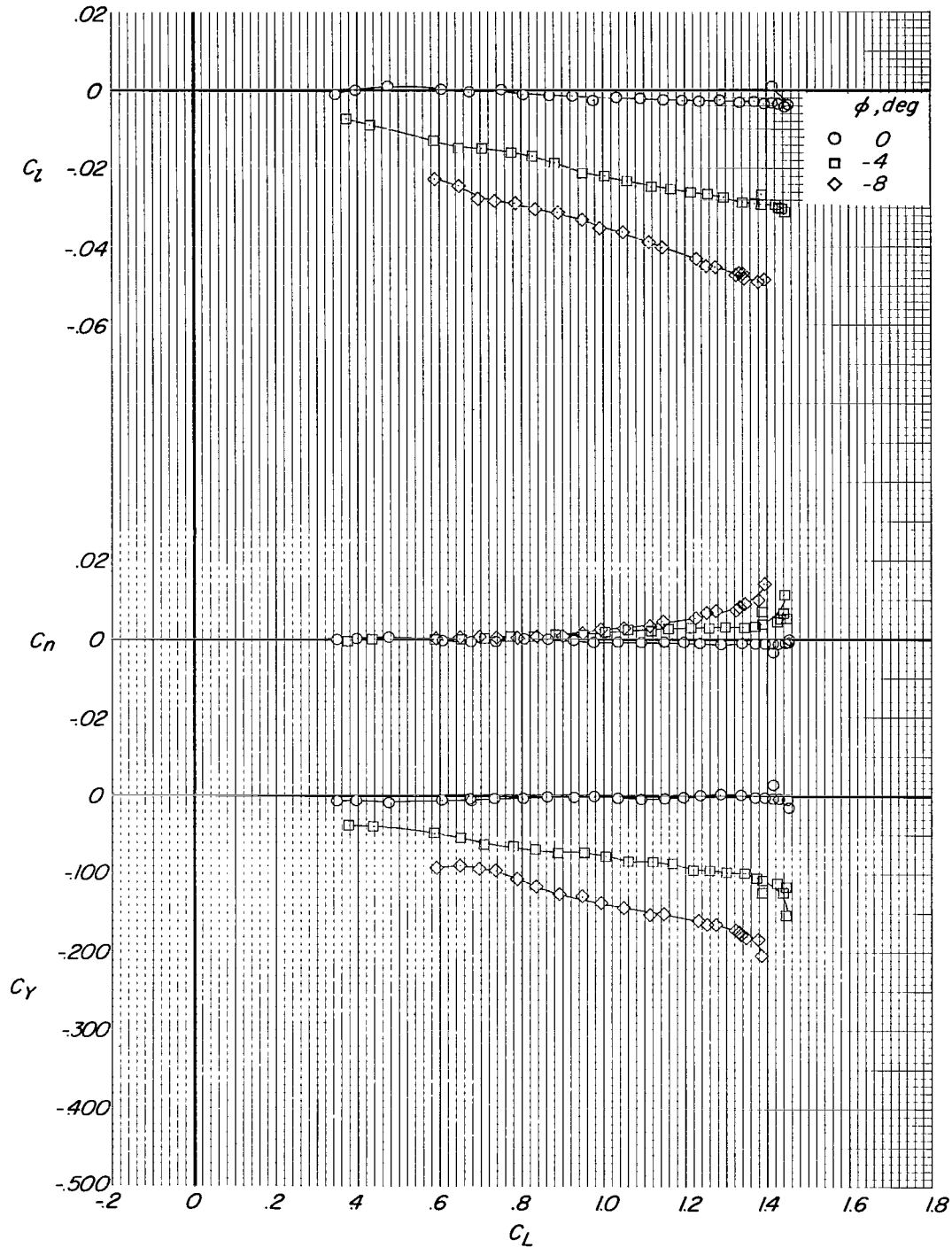

Figure 16.- Effect of wing bank angle on lateral aerodynamic characteristics of model with wing 2. Pivot location is $x/l_k = 0.778$ and $z/\bar{c} = 0.047$. Sideslip angle is 0^o; $i_w = 15^o$; and $q = 958\ N/m^2$ (20.0 lb/ft^2).

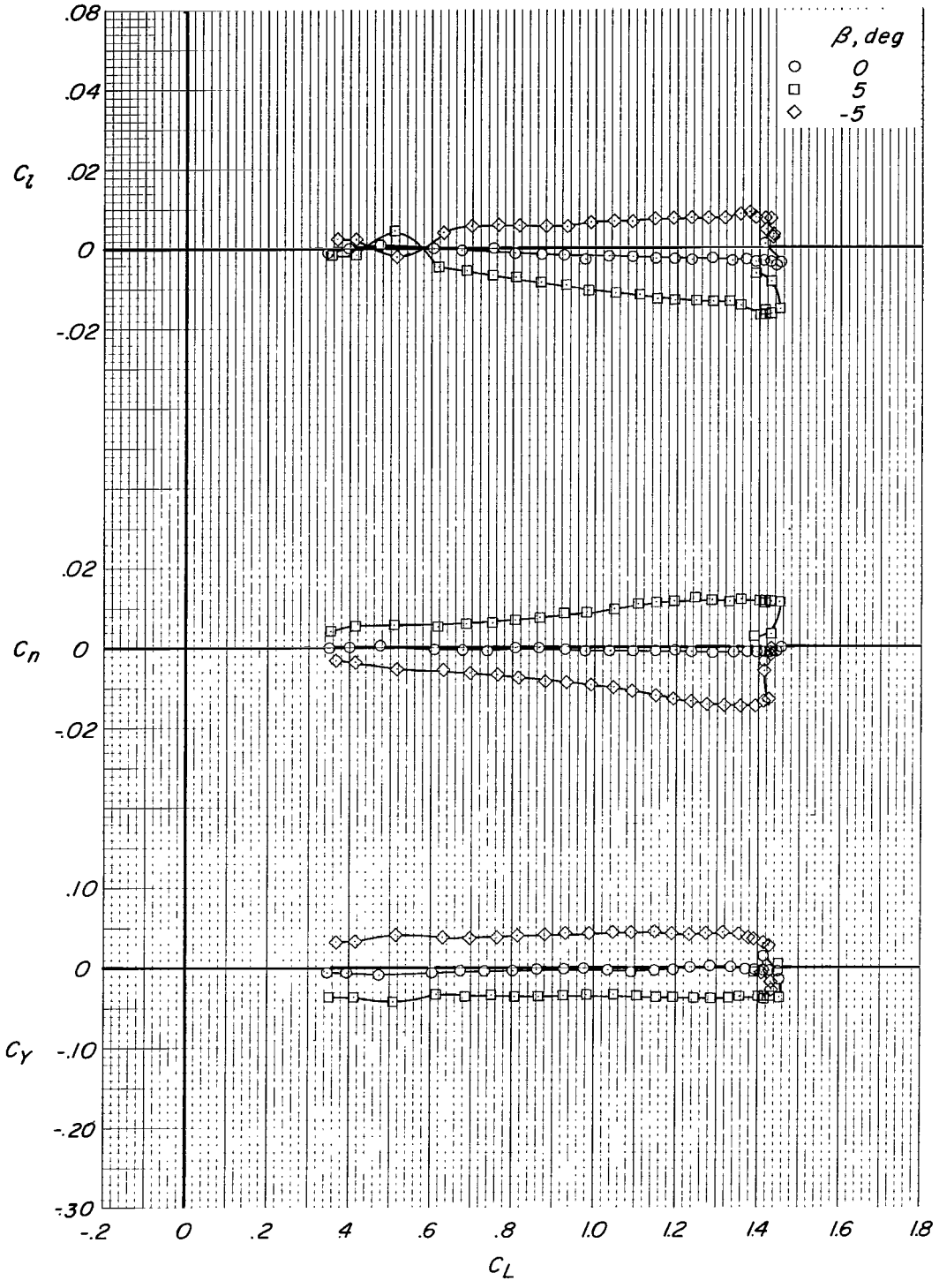

Figure 17.- Effect of sideslip angle on lateral aerodynamic characteristics of model with wing 2. Pivot location is $x/\ell_k = 0.778$ and $z/\bar{c} = 0.047$. Wing bank angle is 0^0; $i_w = 15^0$; and $q = 958\ N/m^2$ (20.0 lb/ft^2).

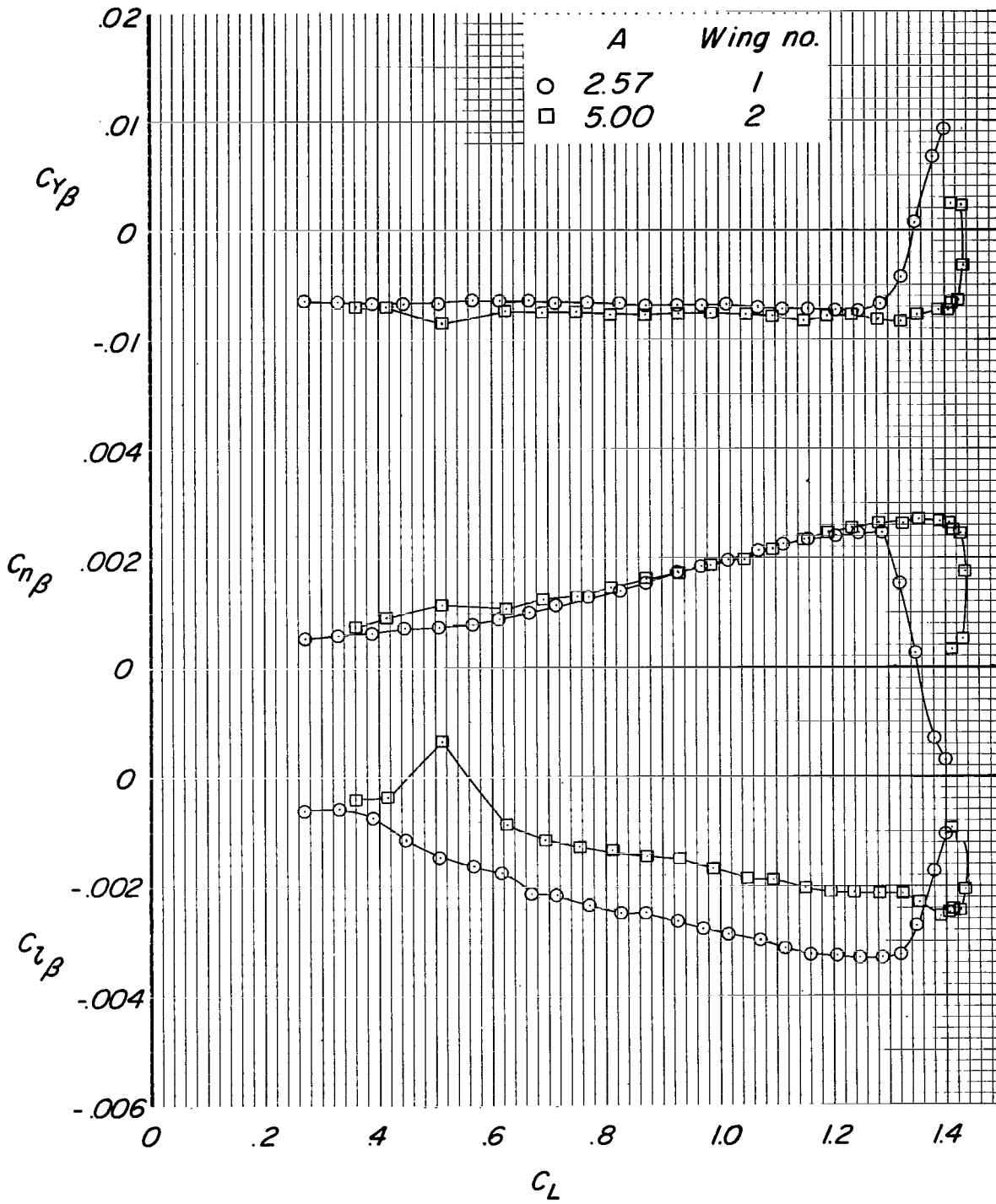

Figure 18.- Effect of aspect ratio on static lateral derivatives for the model. $i_w = 15^o$ and $q = 958\ N/m^2$ (20.0 lb/ft^2). Pivot locations are: Wing 1: $x/l_k = 0.500$, $z/\bar{c} = 0.033$; Wing 2: $x/l_k = 0.778$; $z/\bar{c} = 0.047$.

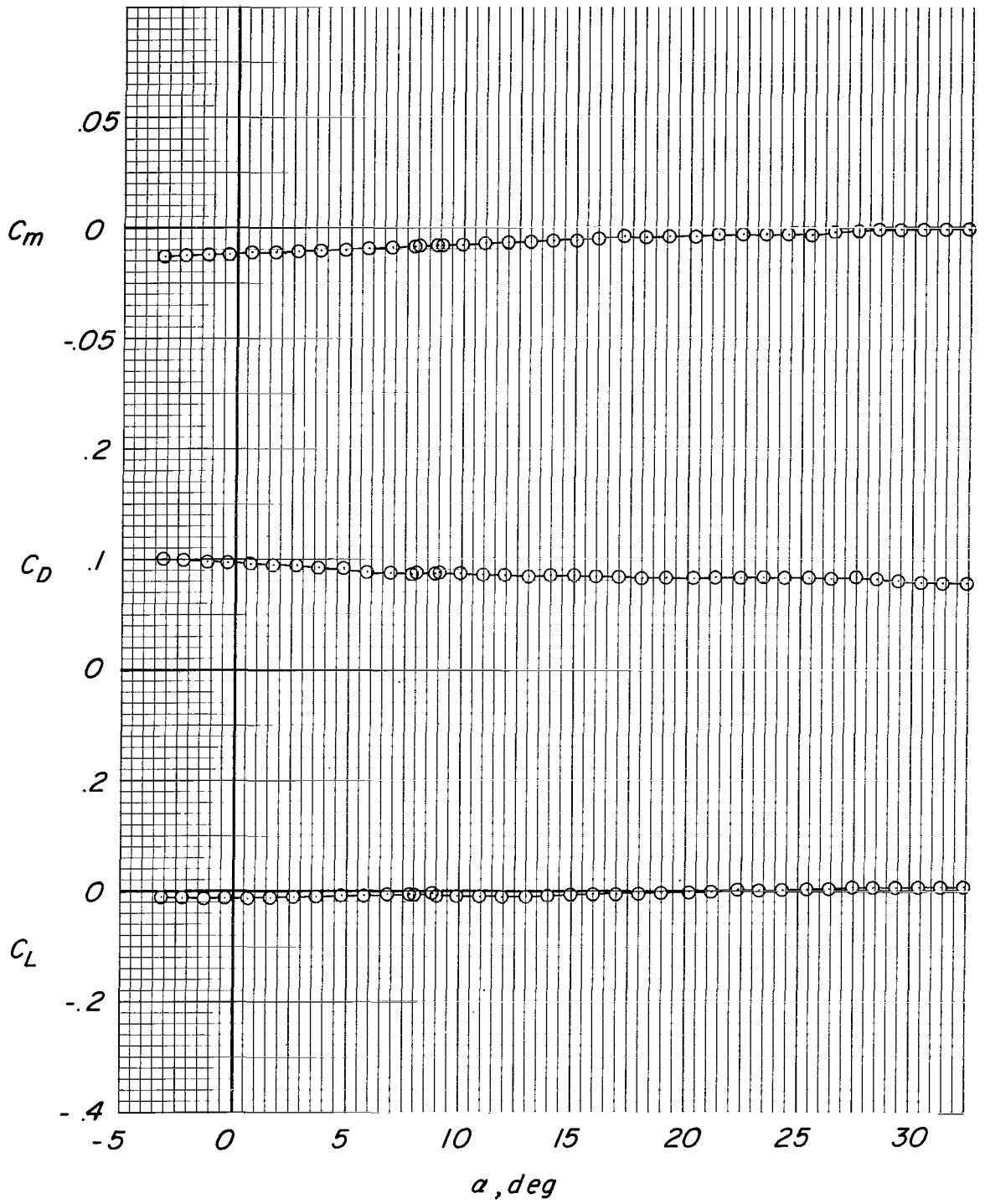

Figure 19.- Longitudinal aerodynamic characteristics of fuselage with wing off. q = 718 N/m^2 (15.0 lb/ft^2). Coefficients are based on wing 1 reference area and chord.

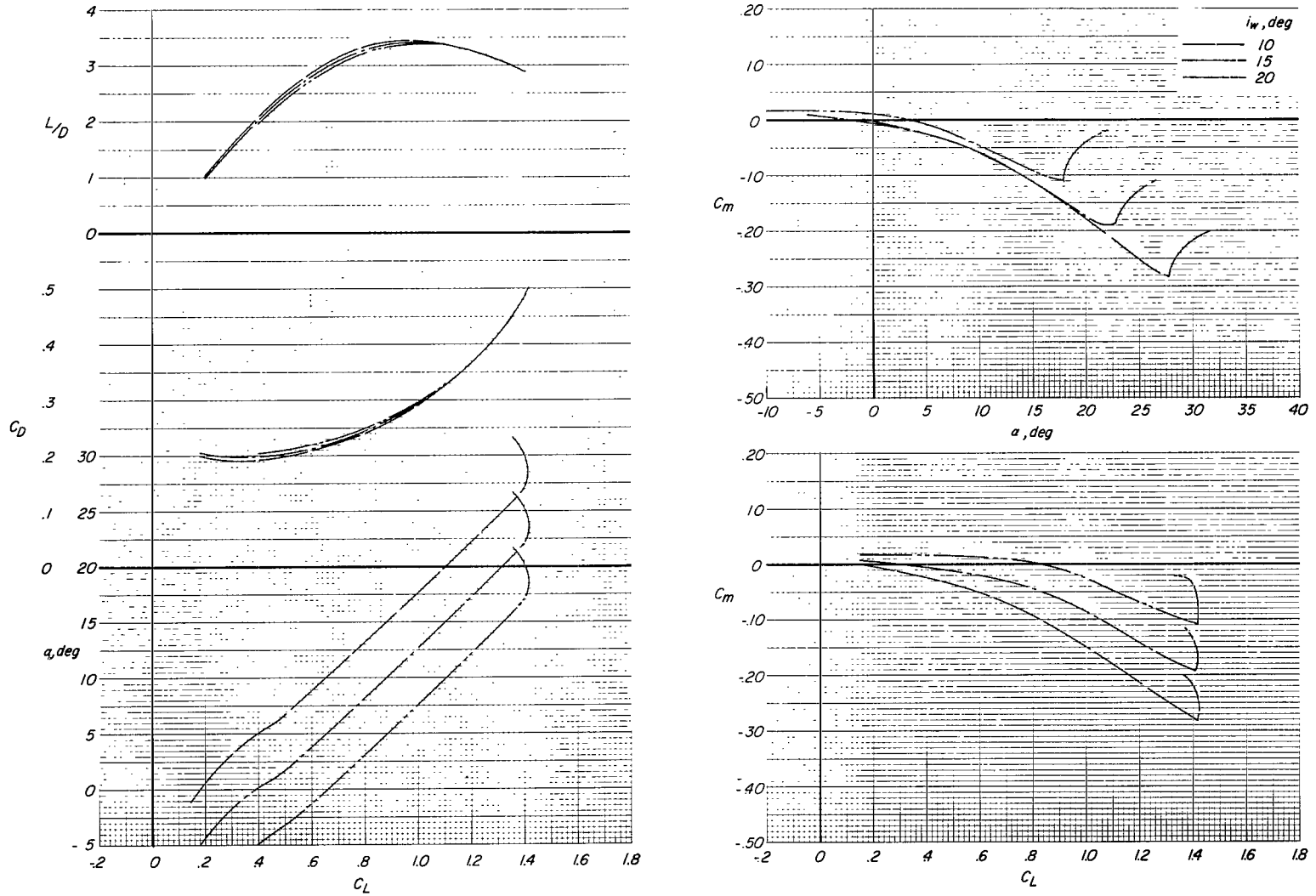

Figure 20.- Effect of wing-fuselage incidence on longitudinal aerodynamic characteristics of model with wing 1. Pivot location is $x/l_k = 0.478$ and $z/\bar{c} = 0.033$. These data obtained from wing-alone and fuselage wing-off data. $q = 718\ N/m^2$ (15.0 lb/ft^2).

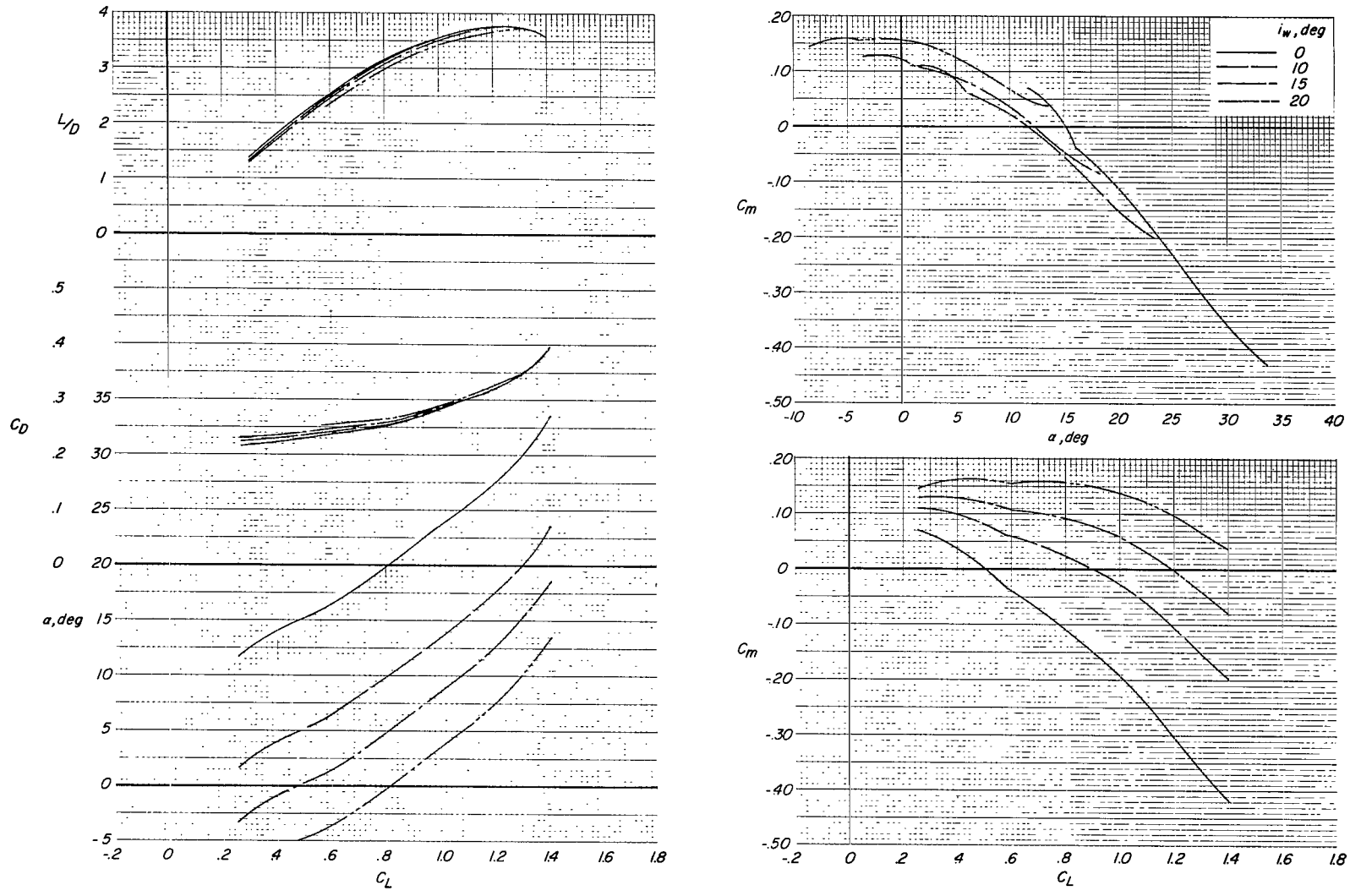

Figure 21.- Effect of wing-fuselage incidence on longitudinal aerodynamic characteristics of model with wing 2. Pivot location is $x/l_k = 0.749$ and $z/\bar{c} = 0.047$. These data obtained from wing-alone and fuselage wing-off data. $q = 718\ N/m^2$ (15.0 lb/ft^2).

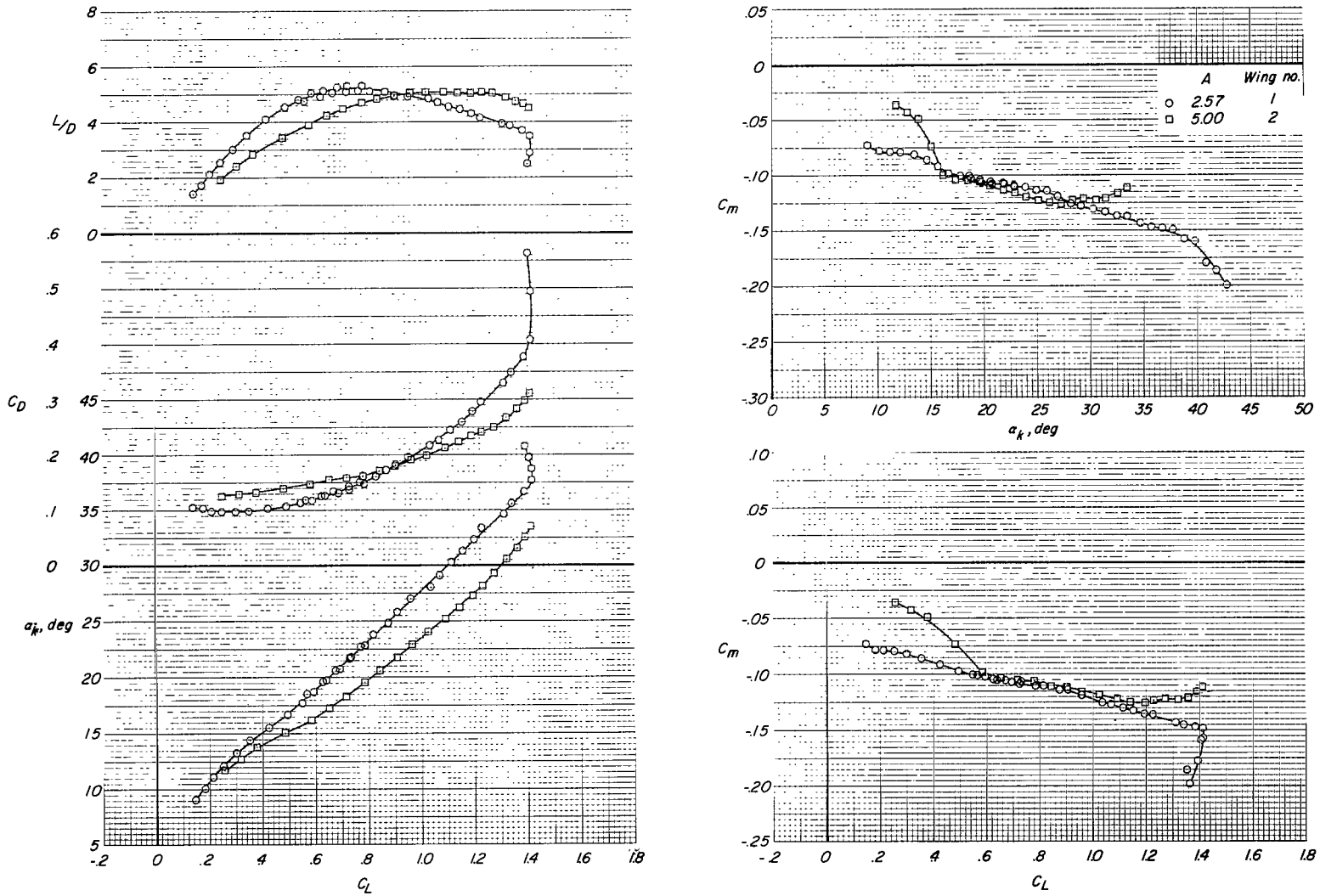

Figure 22.- Longitudinal aerodynamic characteristics of wings 1 and 2 showing effect of aspect ratio.
$q = 718\ N/m^2$ (15.0 lb/ft^2).

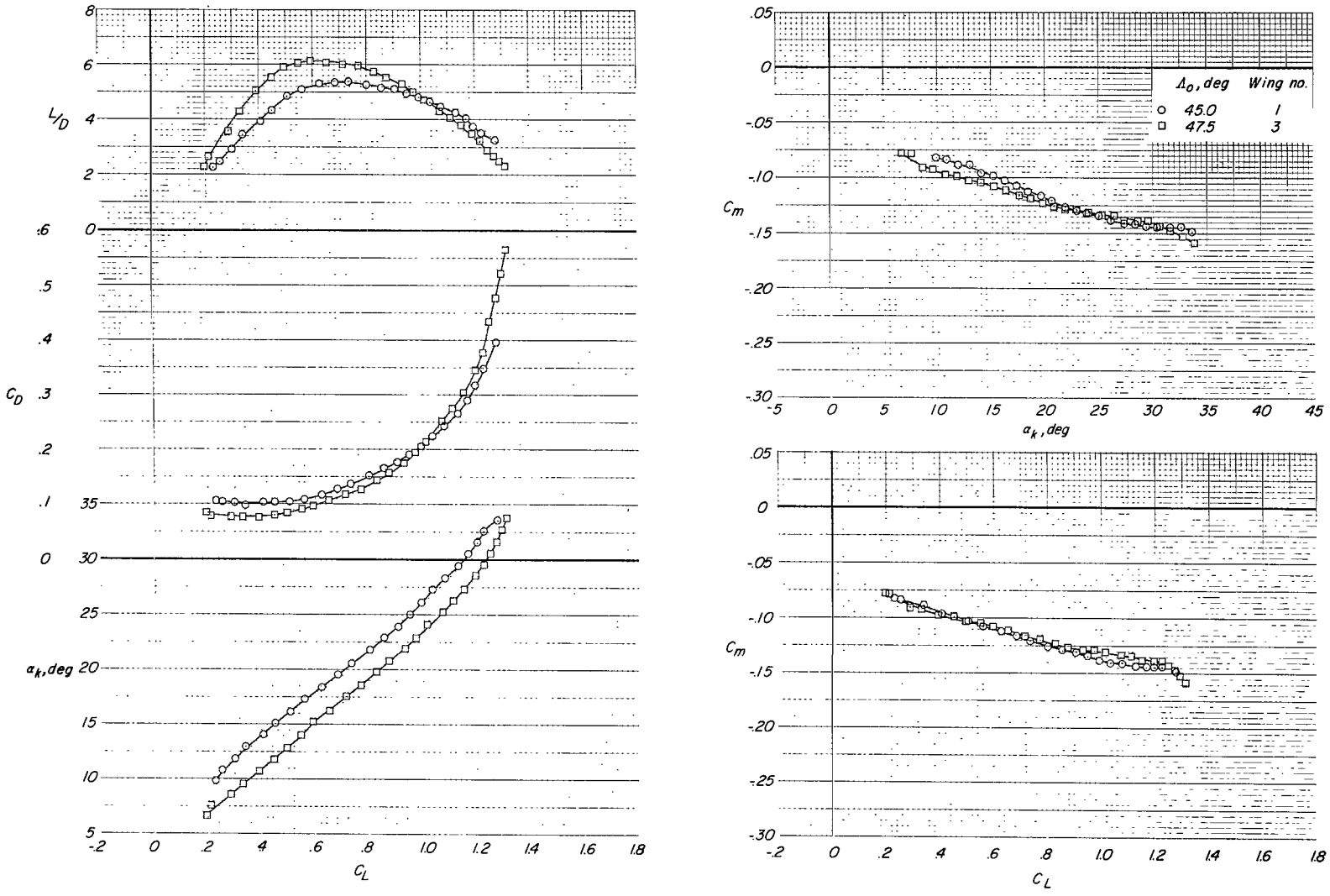

Figure 23.- Longitudinal aerodynamic characteristics of wings 1 and 3 showing effect of flat-pattern sweep. $q = 479\ N/m^2$ (10.0 lb/ft^2).

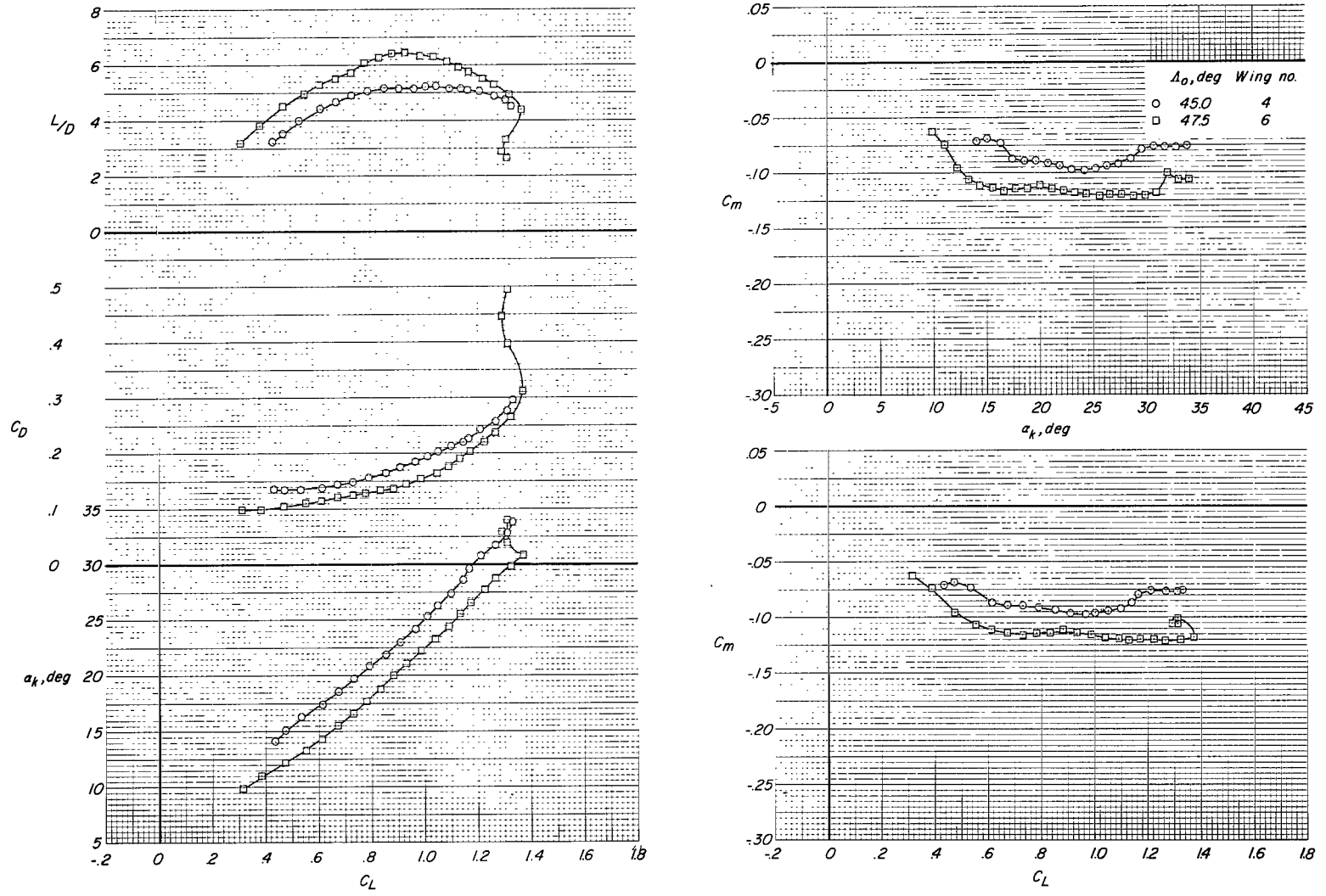

Figure 24.- Longitudinal aerodynamic characteristics of wings 4 and 6 showing effect of flat-pattern sweep.
$q = 479\ N/m^2$ (10.0 lb/ft^2).

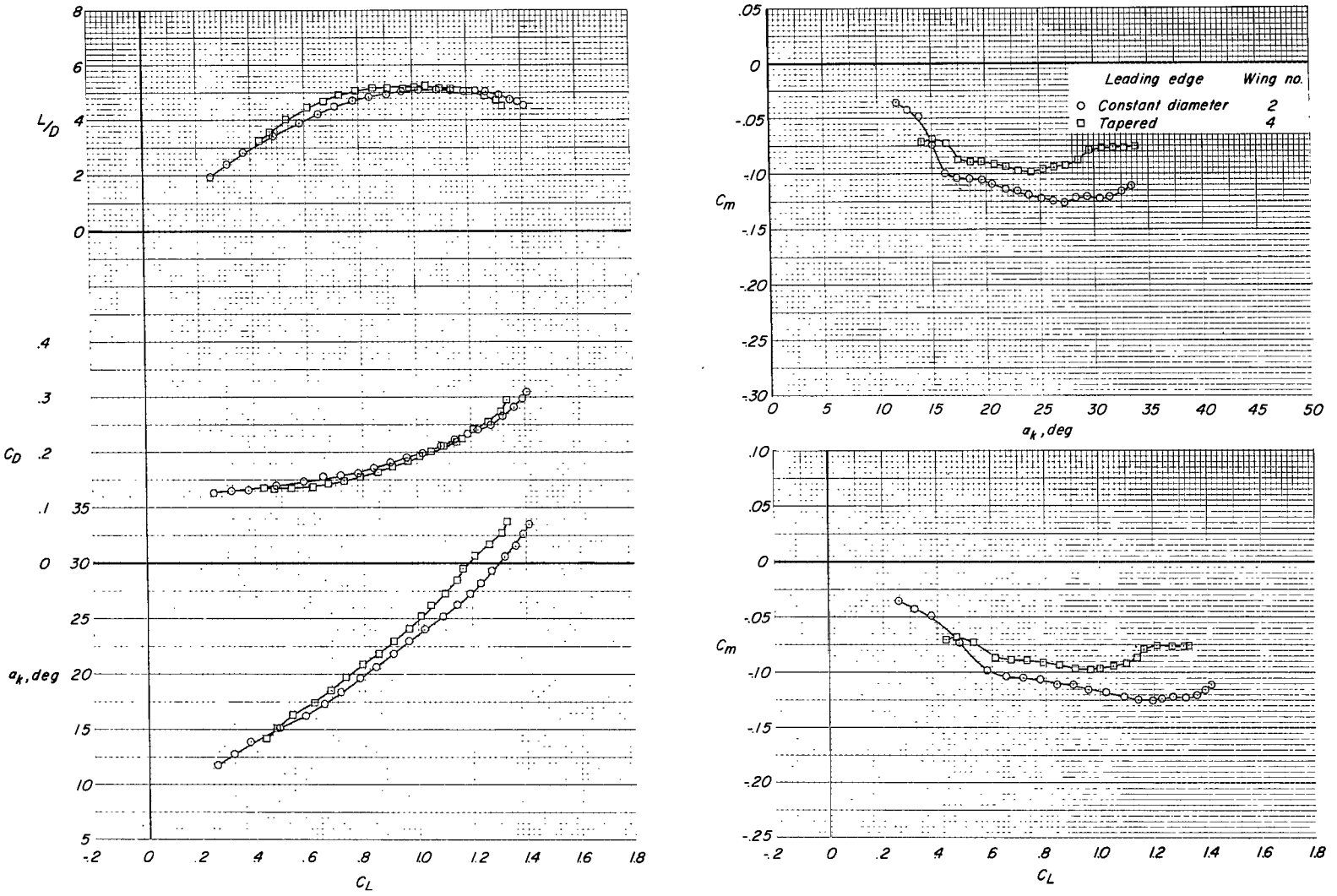

Figure 25.- Longitudinal aerodynamic characteristics of wings 2 and 4 showing effect of leading-edge taper.
$q = 718\ N/m^2$ (15.0 lb/ft^2).

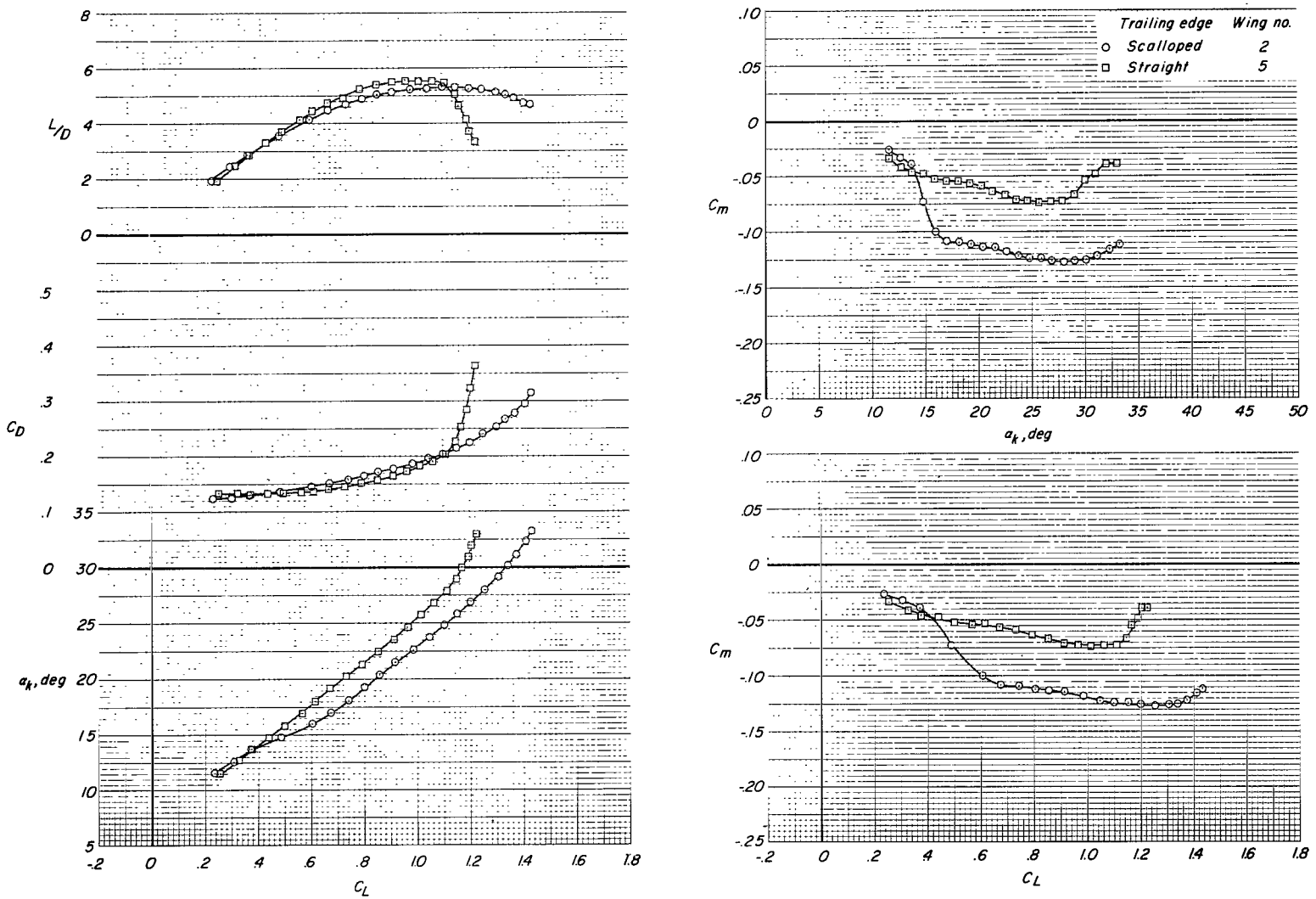

Figure 26.- Longitudinal aerodynamic characteristics of wings 2 and 5 showing effect of trailing-edge scallop.
q = 479 N/m^2 (10.0 lb/ft^2).

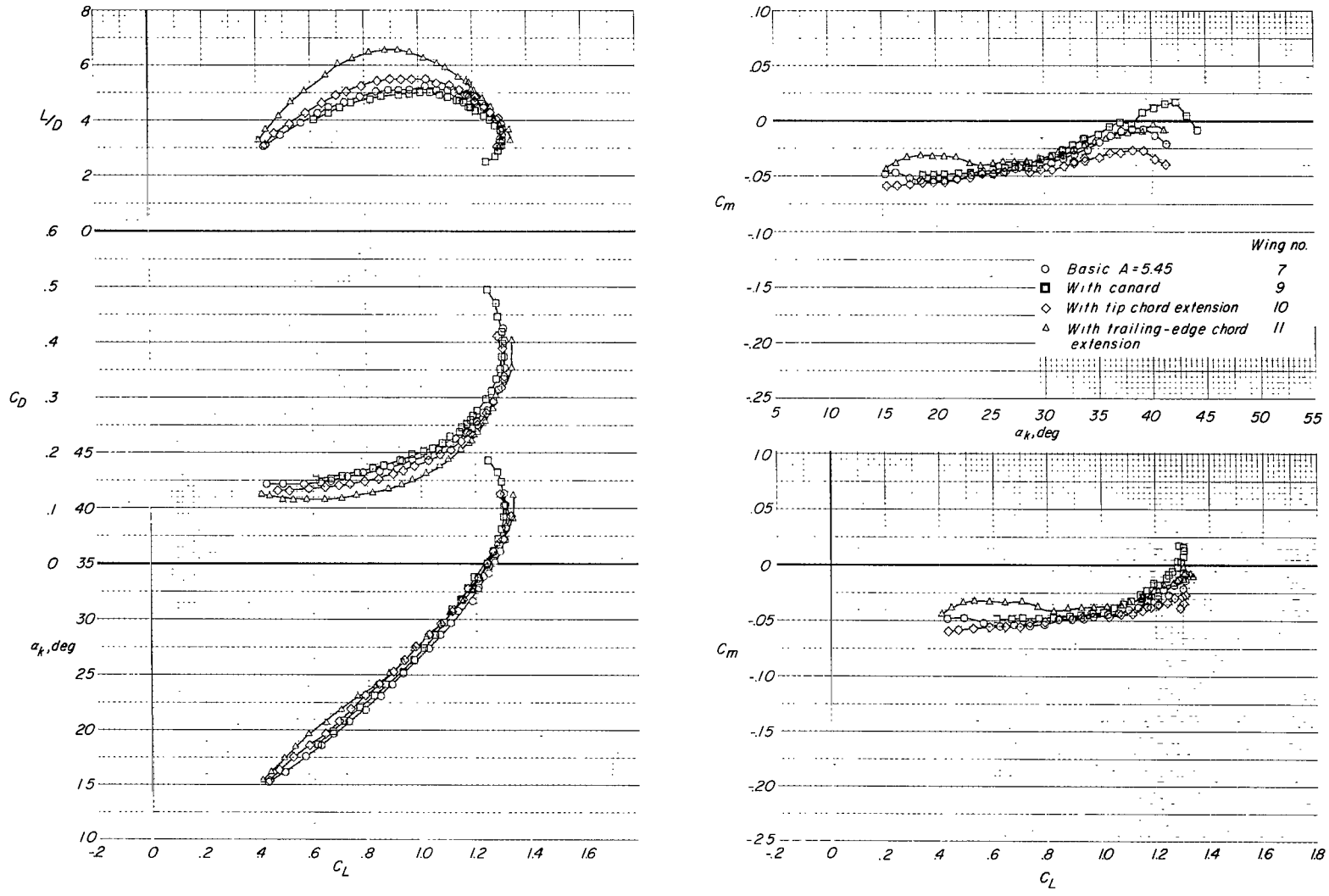

Figure 27.- Longitudinal aerodynamic characteristics of wings 7, 9, 10, and 11 showing effects of modifications of wing 7. q = 479 N/m^2 (10.0 lb/ft2).

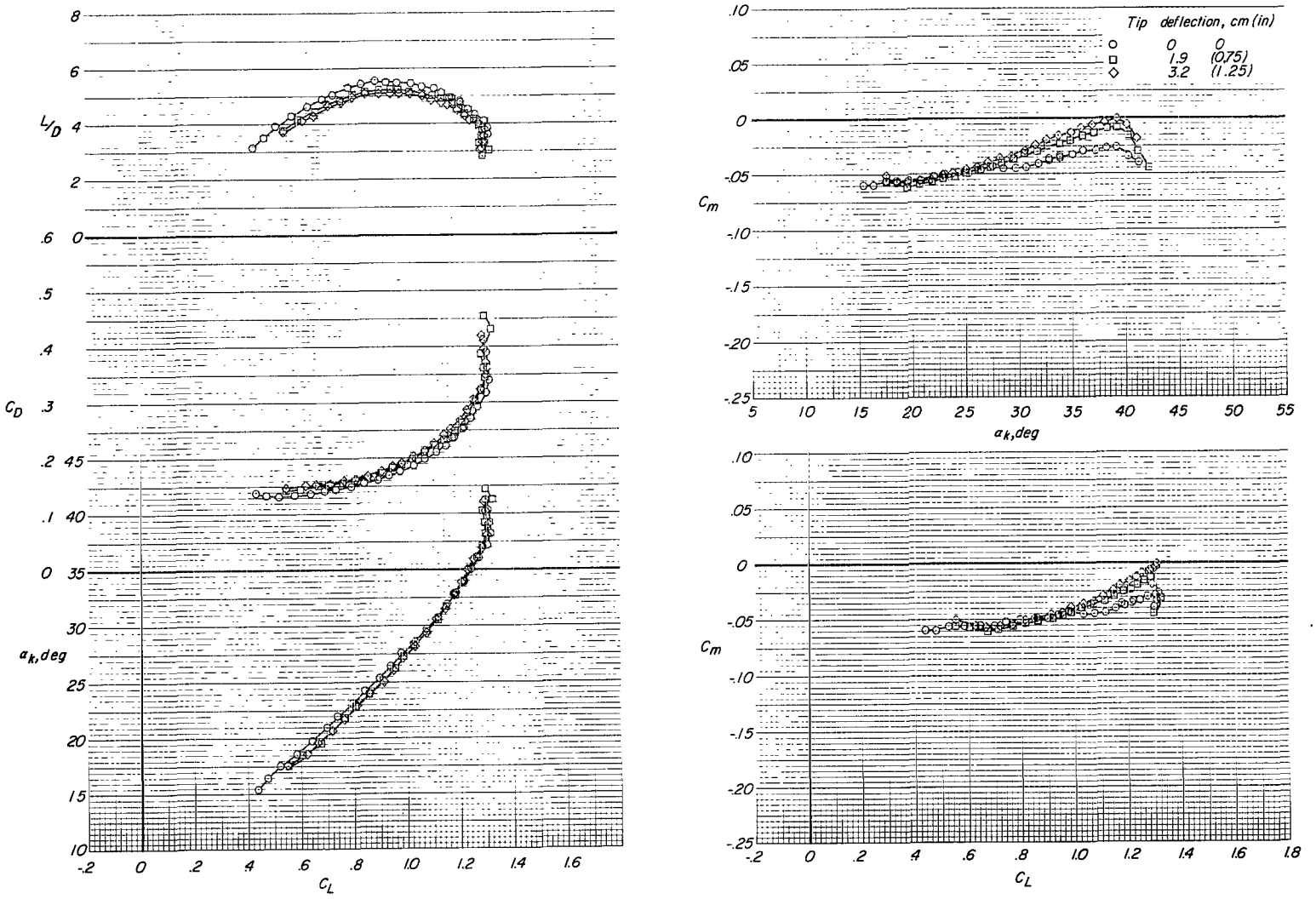

Figure 28.- Longitudinal aerodynamic characteristics of wing 10 showing effect of tip deflection.
$q = 479\ N/m^2$ (10.0 lb/ft^2).

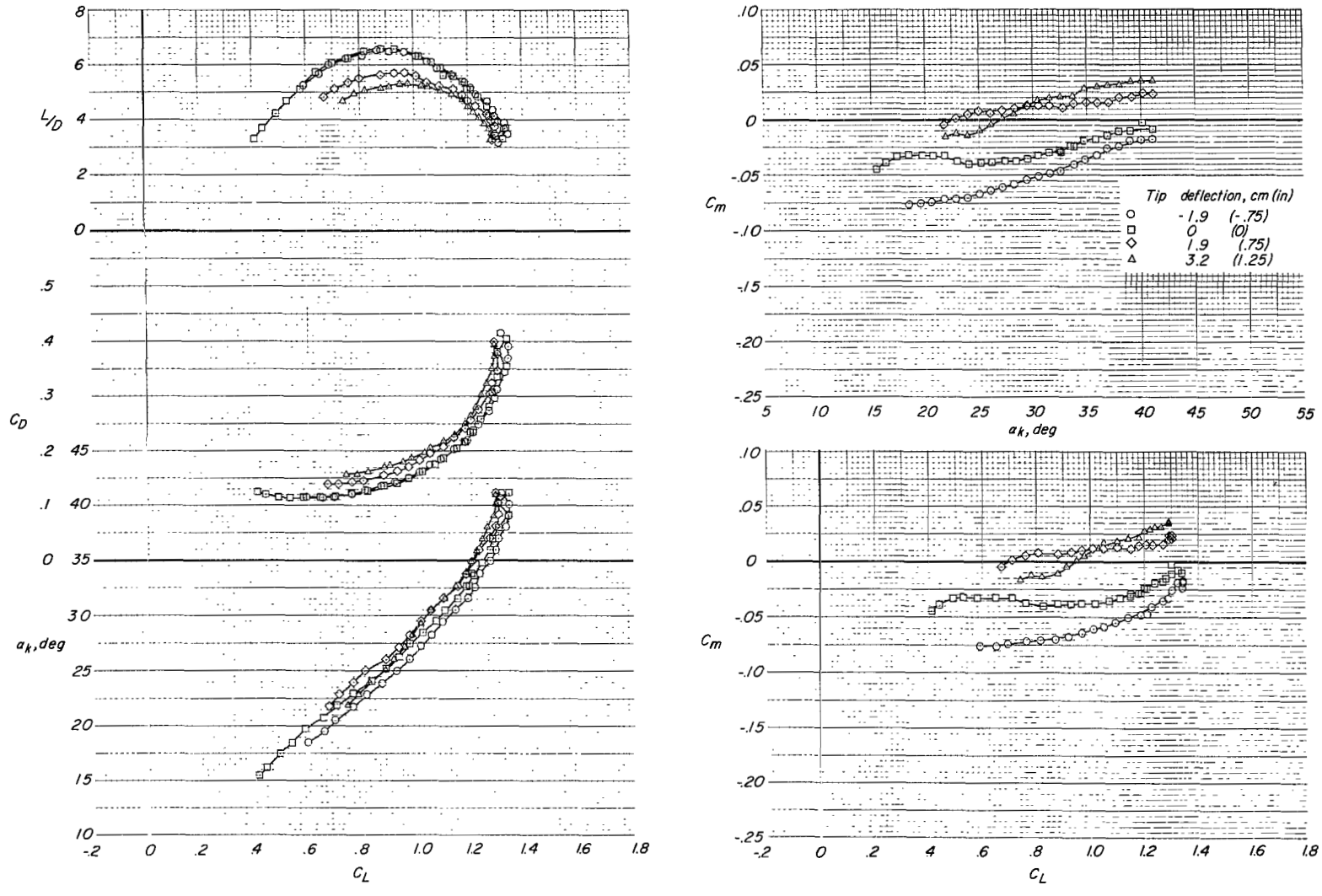

Figure 29.- Longitudinal aerodynamic characteristics of wing 11 showing effect of tip deflection.
$q = 479\ N/m^2$ (10.0 lb/ft^2).

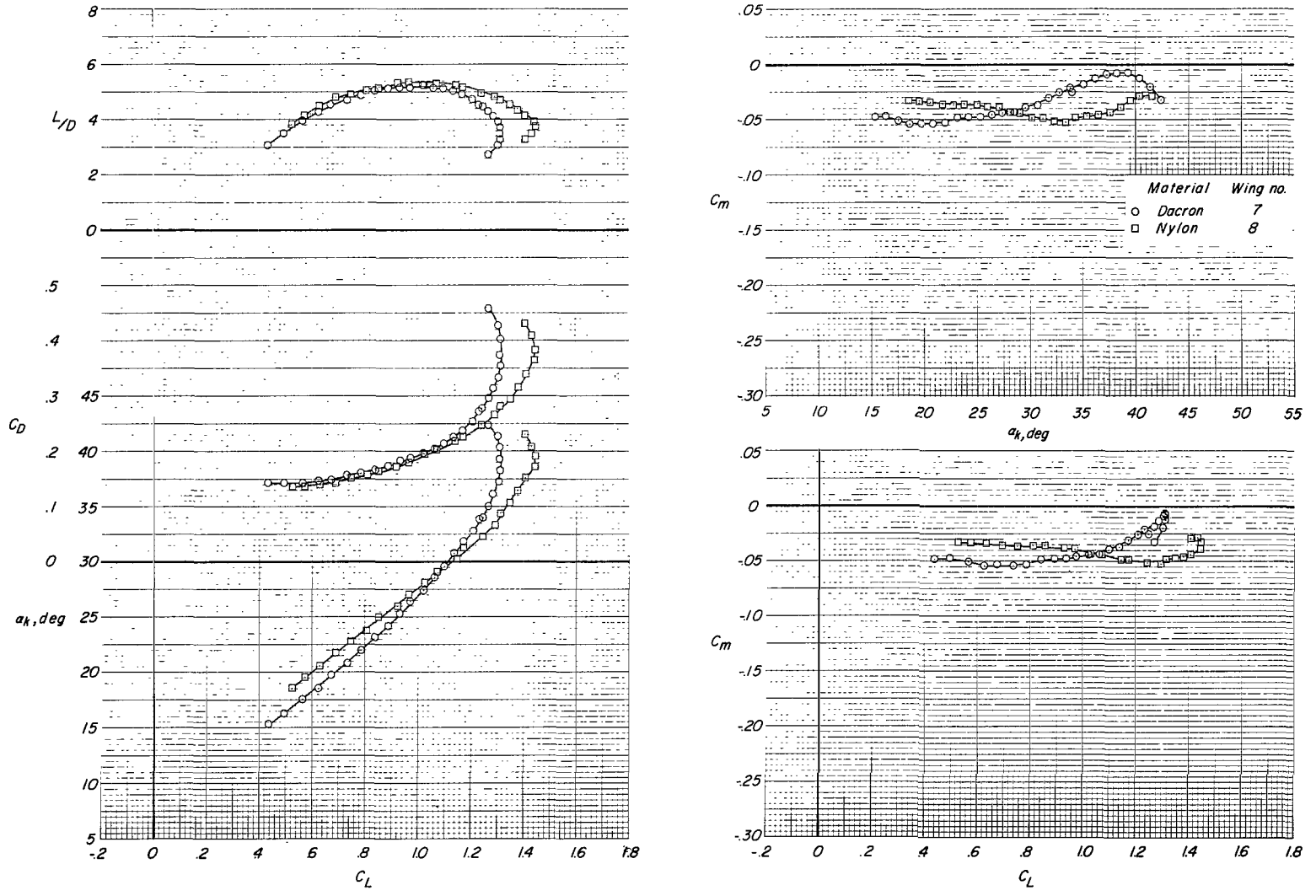

Figure 30.- Longitudinal aerodynamic characteristics of wings 7 and 8 showing effect of canopy material. q = 479 N/m^2 (10.0 lb/ft^2).

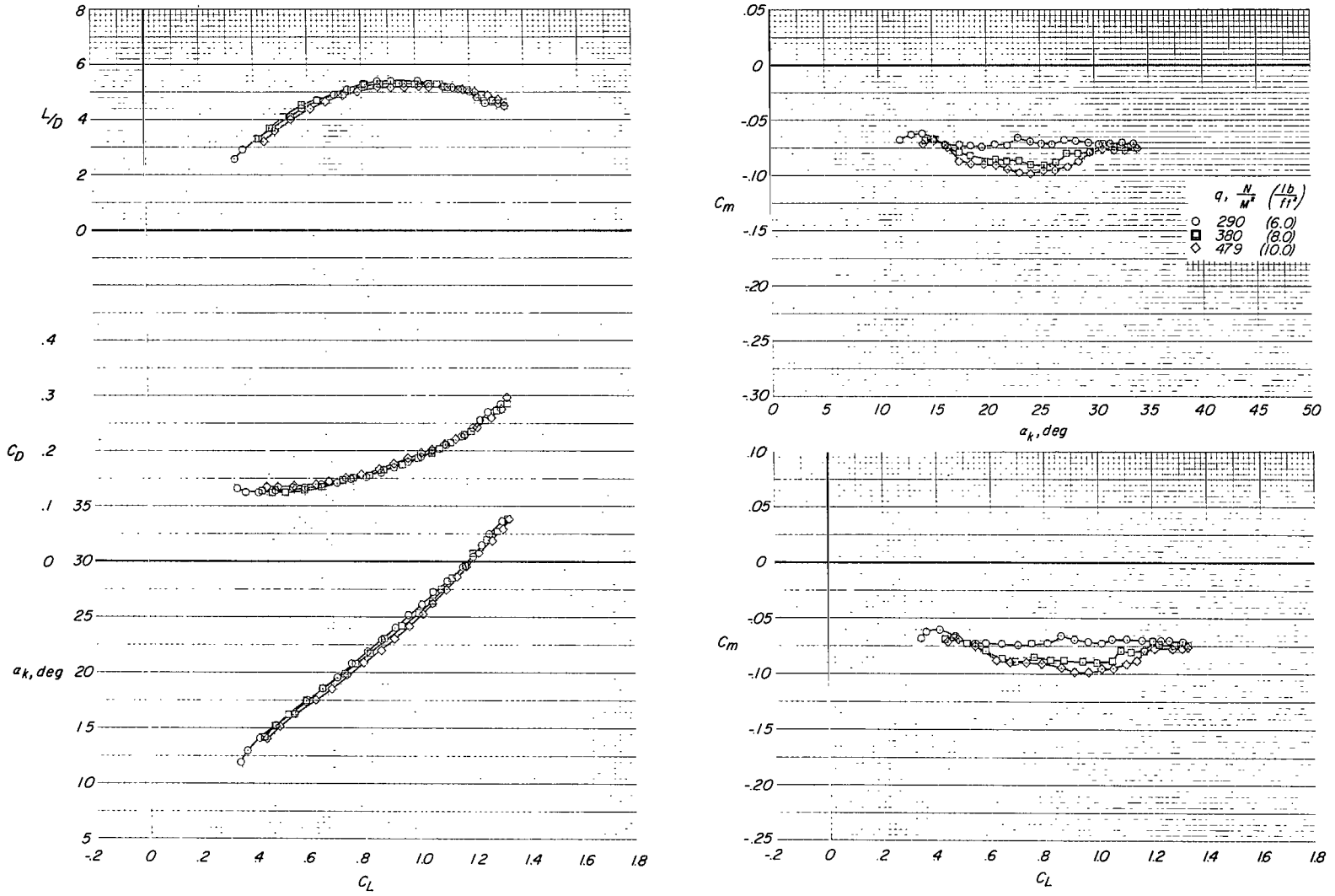

Figure 31.- Longitudinal aerodynamic characteristics of wing 4 showing effect of dynamic pressure.

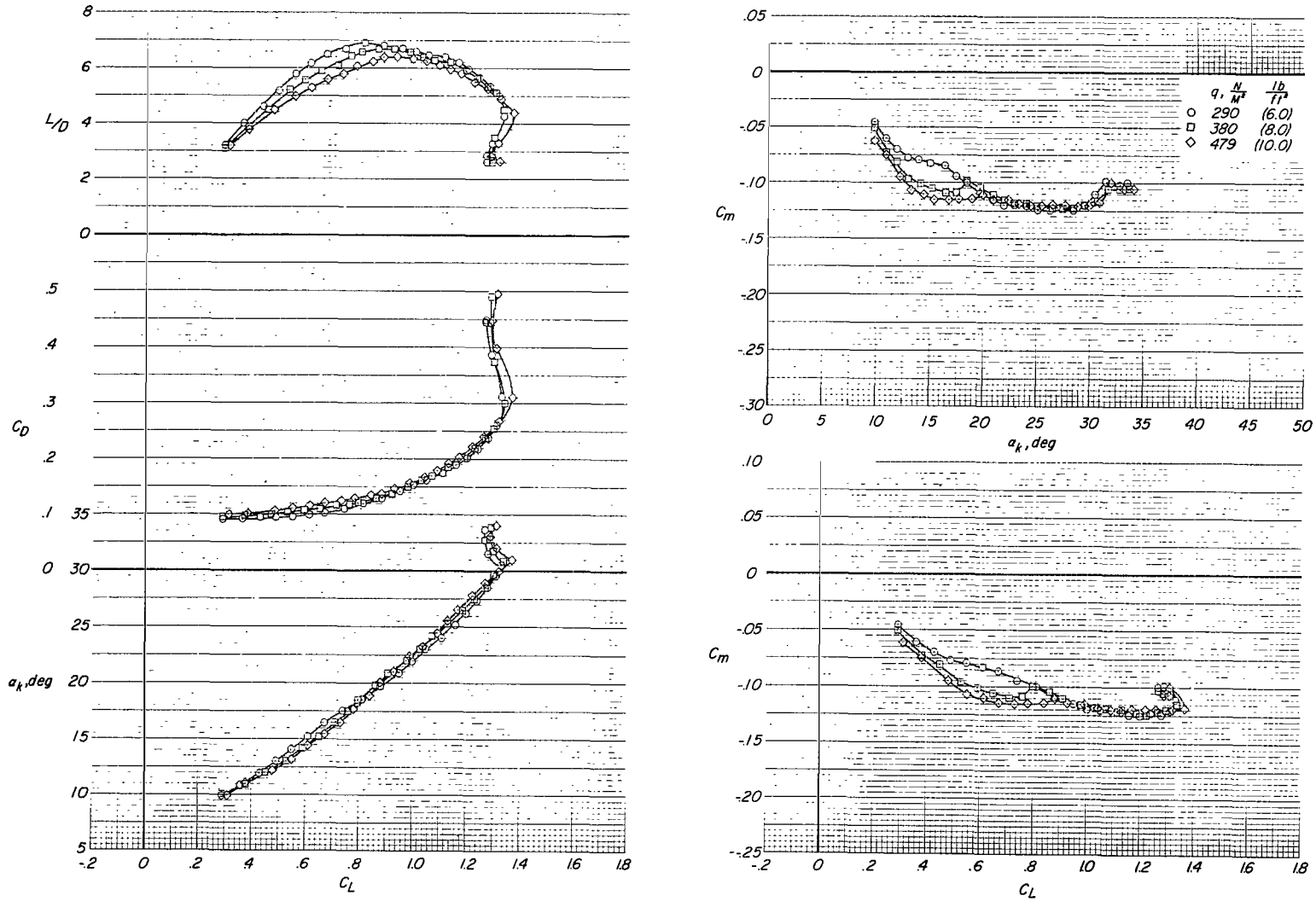

Figure 32.- Longitudinal aerodynamic characteristics of wing 6 showing effect of dynamic pressure.

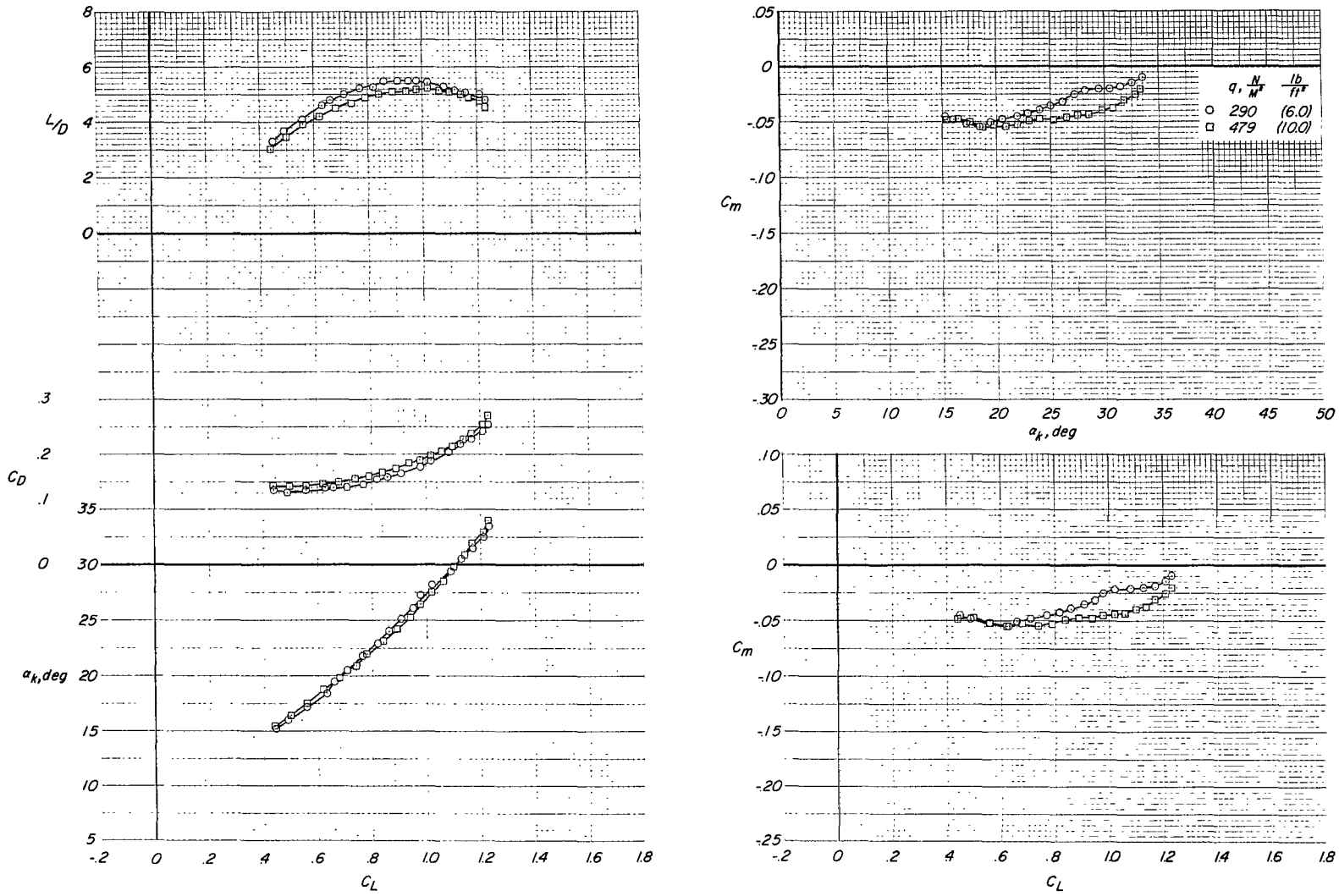

Figure 33.- Longitudinal aerodynamic characteristics of wing 7 showing effect of dynamic pressure.

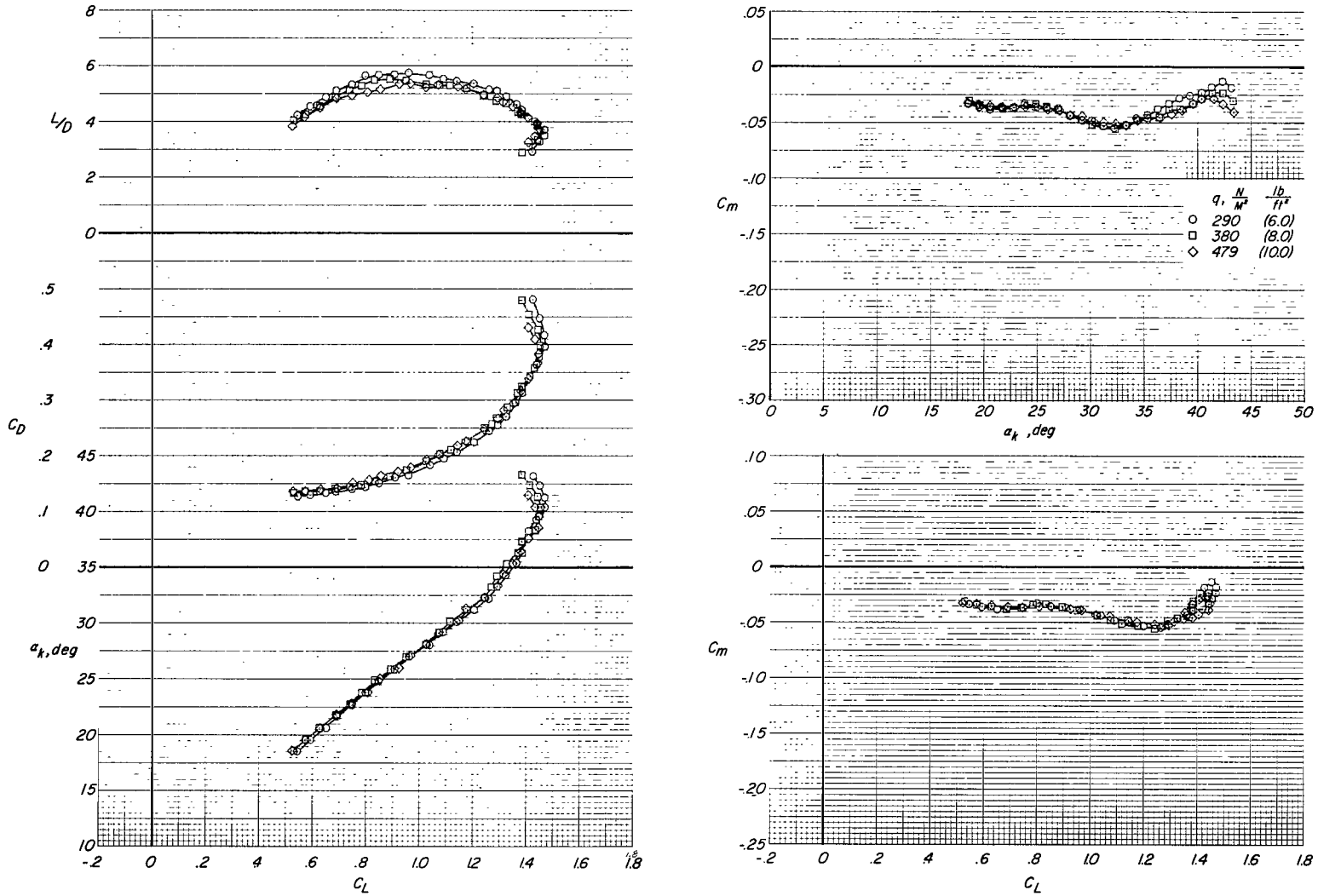

Figure 34.- Longitudinal aerodynamic characteristics of wing 8 showing effect of dynamic pressure.

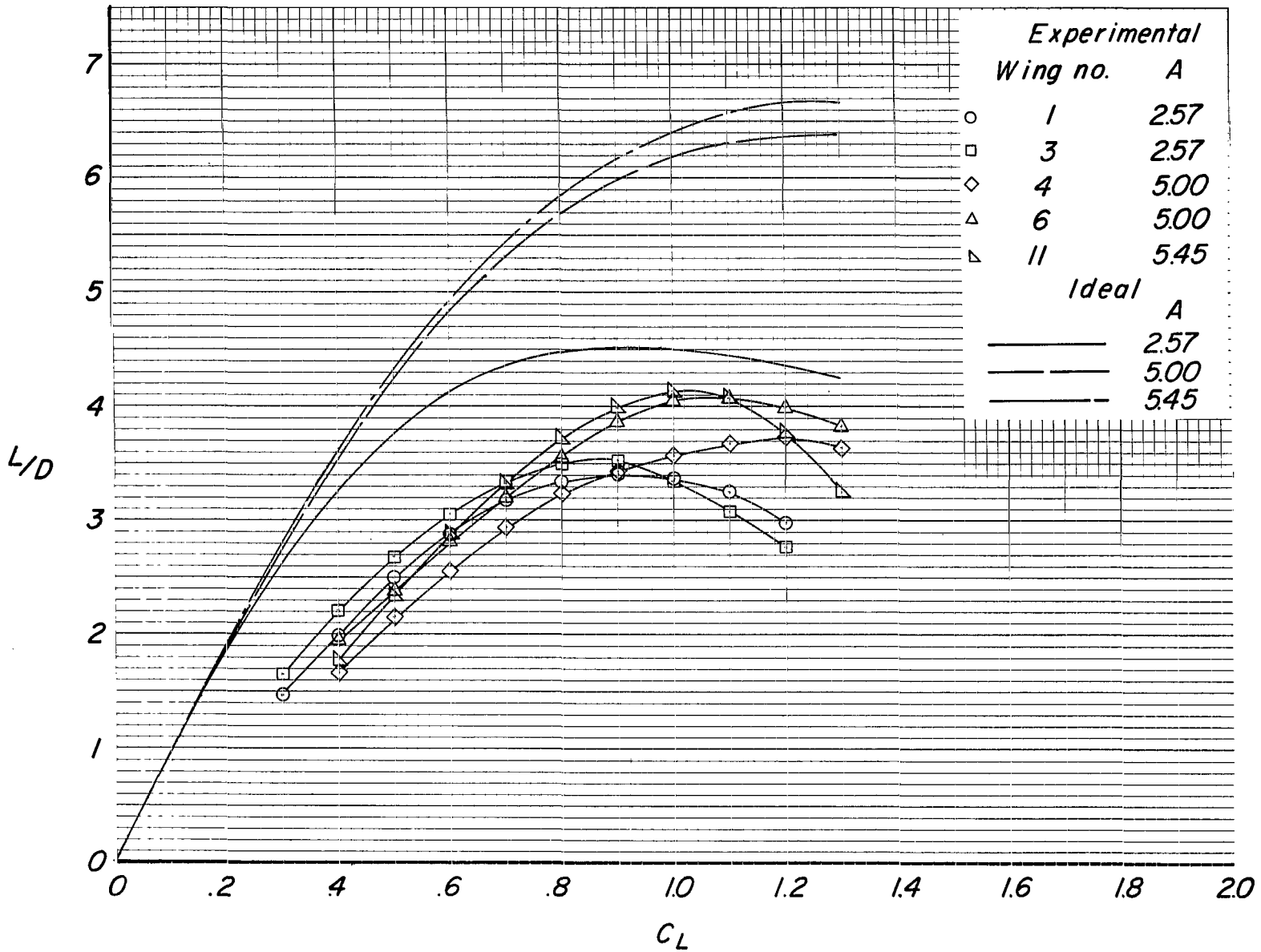

Figure 35.- Aerodynamic performance of model with wings 1, 3, 4, 6, and 11. $q = 479\ N/m^2$ (10.0 lb/ft^2).

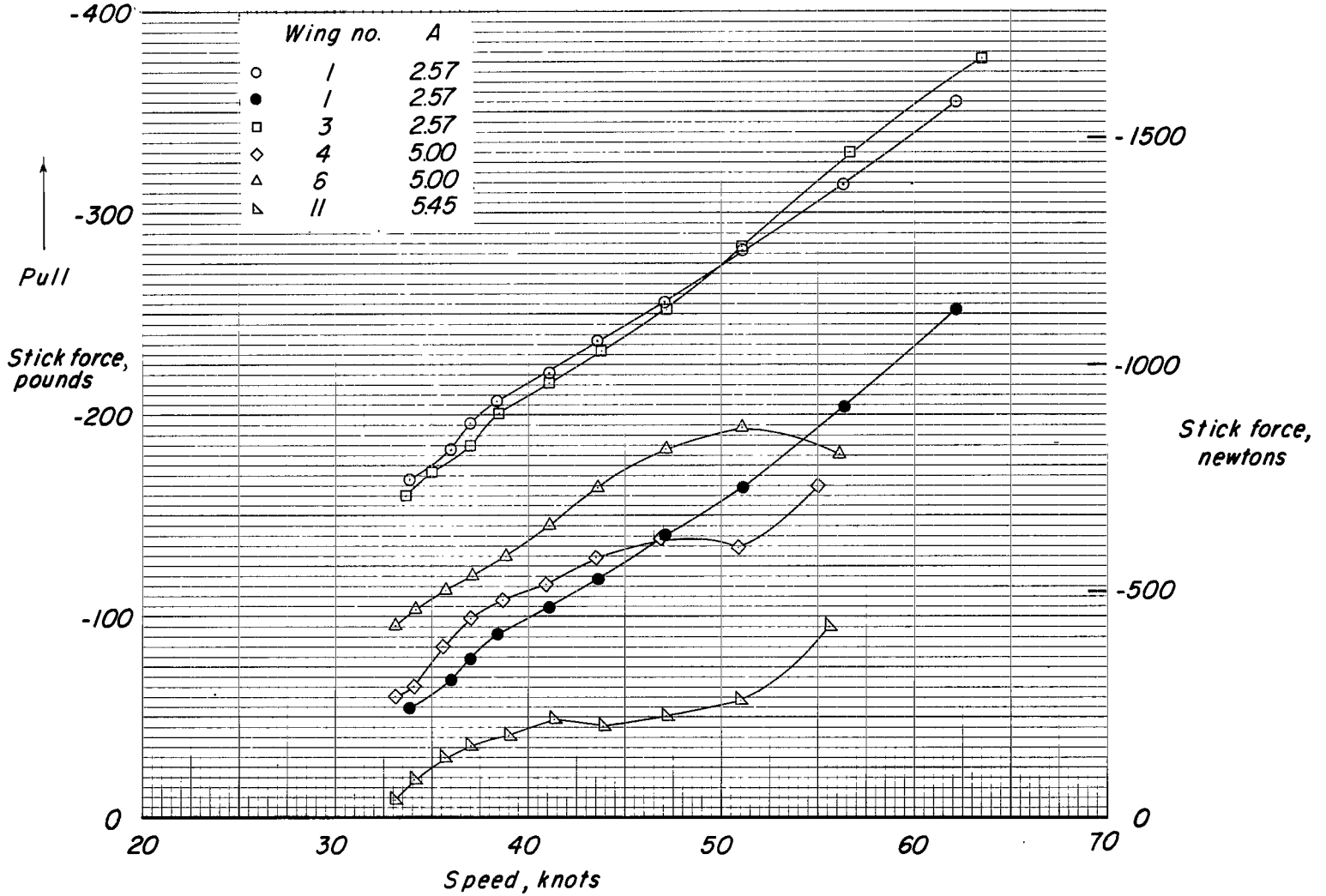

Figure 36.- Stick-force characteristics of model with wings 1, 3, 4, 6, and 11. Pivot is at $\bar{c}/4$ on keel center line except for solid symbols indicating 47.8 percent l_k pivot position.

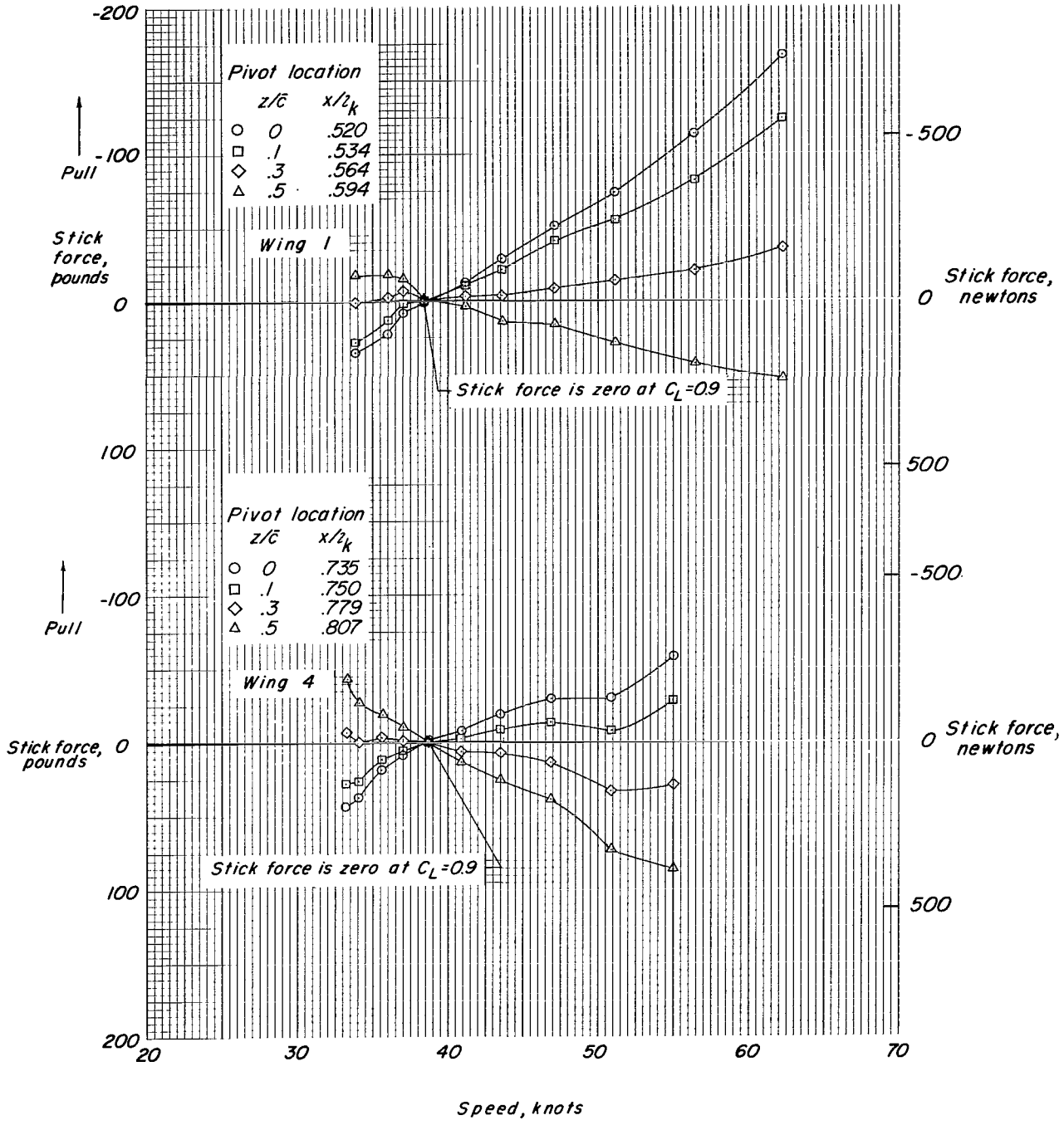

Figure 37.- Effect of distance of pivot point below wing keel on the model stick-force characteristics with zero stick force at $C_L = 0.9$.

NASA-Langley, 1966 L-4797

"The aeronautical and space activities of the United States shall be conducted so as to contribute . . . to the expansion of human knowledge of phenomena in the atmosphere and space. The Administration shall provide for the widest practicable and appropriate dissemination of information concerning its activities and the results thereof."

—NATIONAL AERONAUTICS AND SPACE ACT OF 1958

NASA SCIENTIFIC AND TECHNICAL PUBLICATIONS

TECHNICAL REPORTS: Scientific and technical information considered important, complete, and a lasting contribution to existing knowledge.

TECHNICAL NOTES: Information less broad in scope but nevertheless of importance as a contribution to existing knowledge.

TECHNICAL MEMORANDUMS: Information receiving limited distribution because of preliminary data, security classification, or other reasons.

CONTRACTOR REPORTS: Technical information generated in connection with a NASA contract or grant and released under NASA auspices.

TECHNICAL TRANSLATIONS: Information published in a foreign language considered to merit NASA distribution in English.

TECHNICAL REPRINTS: Information derived from NASA activities and initially published in the form of journal articles.

SPECIAL PUBLICATIONS: Information derived from or of value to NASA activities but not necessarily reporting the results of individual NASA-programmed scientific efforts. Publications include conference proceedings, monographs, data compilations, handbooks, sourcebooks, and special bibliographies.

Details on the availability of these publications may be obtained from:

SCIENTIFIC AND TECHNICAL INFORMATION DIVISION

NATIONAL AERONAUTICS AND SPACE ADMINISTRATION

Washington, D.C. 20546